POLITECNICO DI MILANO
Scuola di Ingegneria Industriale e dell'Informazione
Dipartimento di Scienze e Tecnologie Aerospaziali
Corso di Laurea Magistrale in Ingegneria Aeronautica

Aerodynamic modifications to improve the whirl flutter stability of tiltrotors

Supervisor:
Prof. Giuseppe Quaranta

Master thesis by:
Edoardo Maria Codispoti,
student ID 837567

Academic Year 2016-2017

To my family,
Alessia
and my friends
who always supported me.

Abstract

The whirl flutter is an aeroelastic instability that affects tiltrotors during high speed flights and could reduce their flight envelopes. In this work, the blades are modified to improve the aeroelastic stability of the system. The modification are purely aerodynamic, indeed, the structure is fixed to keep the problem simple. The study is conducted using a multibody semi-model of a tiltrotor based on the well known WRATS model by NASA.

A new solution, gurney flaps, is used. The application of them is done through the aerodynamic coefficients. They have been estimated by curve fitting on experimental data. The method is based on previous works; an extension to estimate the drag coefficient is presented in the thesis. A parametric analysis of the gurney flaps introduction on tiltrotors has been done and reported. The use of gurneys is capable of introducing a beneficial pitching down moment on the blade, however, the rotor torque and the loads increase. An important variation of whirl flutter speed has been found.

The use of advanced geometry blades is studied in detail. Some parametric studies on blades with swept tips, tip anhedral and double sweep angle are provided. Also in this case, there is a general increase of loads and power requirements. The blades with simple swept tips are capable of increasing the whirl flutter speed, instead, the double sweep reduces it as well as the tip with anhedral. The causes of the increase of stability are studied in detail, the application of swept blades and gurney flaps generates an elastic twist down of the blade, reducing the perturbational forces responsible for the whirl flutter. The consequence is an increase of loads.

An optimisation based on a genetic algorithm is set up to combine the effects of the solutions. The fitness function studies the response of the system in the time domain to evaluate an objective value related to the damping. The optimal shape is capable of increasing the whirl flutter speed but increases the loads and the torque of the rotor as well.

Keywords: Aeroelasticity, Tiltrotor, Whirl flutter, Gurney flap.

Sommario

Il whirl flutter è un'instabilità aeroelastica che affligge i tiltrotor durante i voli ad alta velocità e può ridurre il loro inviluppo di volo. In questo lavoro, le pale sono modificate per incrementare la stabilità aeroelastica del sistema. Le modifiche sono solamente aerodinamiche, la struttura non viene modificata per mantenere il problema semplice. Lo studio è condotto usando un semi-modello multicorpo di un tiltrotor basato sul modello WRATS della NASA.

Viene presentata una nuova soluzione basata sui gurney flaps. L'introduzione di questi viene effettuata attraverso i coefficienti aerodinamici. Essi sono stati stimati con il metodo, sviluppato in lavori precedenti, del curve fitting sui dati sperimentali. Un'estensione al coefficiente di resistenza è presentata nella tesi. E' stato eseguito uno studio parametrico dell'applicazione dei gurney flaps sul tiltrotor e i risultati vengono discussi. L'utilizzo di questo apparato genera un vantaggioso momento aerodinamico a picchiare sulle pale, tuttavia, vi è un aumento dei carichi e della coppia del rotore. E' stato trovato un importante incremento di velocità di whirl flutter.

L'utilizzo di pale con geometria avanzata è studiato nel dettaglio. Sono stati effettuati degli studi parametrici sulle pale con freccia in estremità, angolo diedro e doppia freccia, e vengono qui riportati. Anche in questo caso vi è un aumento dei carichi e della potenza necessaria. Le pale con freccia in estremità incrementano la velocità di flutter, invece, le pale con doppia freccia e con angolo diedro la riducono. Le cause dell'aumento di stabilità sono studiate nel dettaglio. L'applicazione della freccia e dei gurney flaps genera una torsione della pala, riducendo le forze aerodinamiche responsabili del whirl flutter. La conseguenza è un aumento dei carichi.

E' stata eseguita un'ottimizzazione basata su un algoritmo genetico per combinare gli effetti delle soluzioni adottate. La funzione di fitness studia la risposta del sistema nel dominio del tempo per valutare un obiettivo collegato con lo smorzamento. La geometria ottima è capace di incrementare la velocità di whirl flutter ma aumentano sia i carichi che la coppia del rotore.

Parole chiave: Aeroelasticità, Tiltrotor, Whirl flutter, Gurney flap.

Acknoledgements

I would like to express my gratitude to my family and friends, who always supported me.

Special thanks to my advisor Giuseppe Quaranta, who helped me to find such as interesting subject and supported me in this work.

Indice

I

Elenco delle figure

Elenco delle tabelle

List of Symbols

c   chord

C_D drag coefficient

C_L lift coefficient

C_M pitching moment coefficient

h   gurney flap height

D   aerodynamic drag

L   lift

M   aerodynamic pitching moment

R   rotor radius

q   dynamic pressure

α angle of attack

α_0 zero-lift angle of attack

Γ anhedral angle

θ_0 collective pitch angle at blade root

λ_i sweep angle i

Introduction

The research of an aircraft with Vertical Takeoff and Landing (VTOL) capabilities triggered the imagination of designer and inventors to produce numerous configurations using a wide variety of lifting and propulsion devices. The predecessor of modern helicopters can be found in the Renaissance thanks to the work of Leonardo Da Vinci. Despite the Da Vinci's machine would not have been able to takeoff due to weight constrictions, the idea of having a large surface to produce enough lift to flight was already understood. Many years later, this elementary concept leads to the definition of the disc loading parameter (is commonly defined as the thrust divided by the area over which it is produced [13]). VTOL vehicles that have a low disc loading require low power per unit of thrust produced, the fuel consumption is lower than the same aircraft but with higher disc loading [16]. Helicopters seem to be the right choice thanks to their large rotors which imply very low disc loading. The main rotors of helicopters provide the thrust to liftoff and to maintain hover conditions balancing the weight. Indeed, in forward flight the thrust produced by the main rotor is used to balance the weight and as propulsive force to win the drag. However, there are important limitations in forward flight that restrict the flight envelope and so their use. Since the rotor encounters an asymmetrical velocity in forward flight, some aerodynamic limitations affect the blades. Stall on the retreating blade and power loss due to compressibility on advancing blade reduce the performance in terms of range and cruise speed. In order to overcome this limitations unconventional configurations arisen. Tiltrotors were born.

The tiltrotor aircraft

The tiltrotor aircraft combines the advantages of VTOL capabilities with the forward speed, range and service ceiling of a fixed turboprop vehicle. The general layout is similar to a conventional aircraft but it mounts large helicopter-like rotors and turboshaft engines at the wing tips. The rotor-engine set can tilt from helicopter mode, with the shafts in vertical direction, to airplane mode, with the shafts in horizontal direction, and vice versa. Tiltrotors allow runway independent operations, and also high speed, long ran-

1

ge flight capabilities. They can perform the same point-to-point operations than an helicopter but flying at higher speeds.

Brief history

The first tiltrotor was the Transcendental Model 1-G in the 1954. It was a single seat, single engine aircraft equipped with two three-blade contra-rotating rotor at the wing tips. The United States Air Force (USAF) financed the Transcendental Aircraft company for the Model 1-g and its successor Model 2. However, the US Government funds were moved to the Bell XV-3 program, causing the abandon of the Model 2. The Bell XV-3 was the first tiltrotor that accomplished the full conversion. It was the proof that tiltrotors work even if with low performances. Like the Model 1-g, the single-engine was mounted in the fuselage, and only the rotor set could rotate. It accomplished 110 transitions between December 1958 and July 1962. Then the last prototype was severely damaged in a wind tunnel accident on May 1966. For this reason the XV-3 program was ended.

Figura 1: Trascendental Model 1-G   Figura 2: Bell XV-3

In 1972 a new program, the XV-15, was funded by NASA, U.S. Army and Bell Helicopter. Thanks to the experience in the XV-3, the XV-15 reached higher performances exploring the possible flight envelope of a tiltrotor. Peculiar differences could be found with respect to the XV-3: instead of a single piston engine configuration, the XV-15 was equipped with two turbo-shaft engines mounted at the wing tips. The new configuration permitted to reach higher velocities and to reduce the complexity of the gearboxes and the transfer of power. Indeed, in the single engine configuration, most of the problems came from the design of the shaft that from the engine reached the propellers; high power and torque have to be transfered for long distances, making the shafts heavy. In the XV-15 configuration, there was still a drive-shaft along the wings for emergency use to transfer power to the opposite rotor in case of engine failure, but that shaft did not normally carry any power load, making it lighter. This new way to deliver power to rotors is still implemented in current tiltrotors. The XV-15 was used as bench test to support the V-22 Osprey military tiltrotor program and the Bell/Agusta (later Leonardo) BA609 (later AW609) civilian tiltrotor.

Figura 3: Bell Boeing V-22 Osprey

Figura 4: Leonardo Elicotteri AW609

The Bell Boeing V-22 Osprey is an American multi-mission military aircraft that first flew in 1989. The peculiarities of tiltrotors plus the folding wings and propellers allowed the U.S. Marine to substitute the Boeing Vertol CH-46 Sea Knight. The successor of the V-22 Osprey is nowadays in development by Bell Helicopter, the name is V-280 Valor. The latter has a little difference with respect to the other tiltrotors, the engines, still located at wing tips, do not rotate but only the rotor can rotate. The Leonardo AW609 is intended to be the first civilian tiltrotor. The AW609 drew on experience gained from Bell's earlier tiltrotors but there are much differences from predecessors. It's the first tiltrotor with a pressurized cabin. It can accommodate up to 9 passengers, and for increased passengers comfort the cabin is also equipped with soundproofing. Thanks to the AW609, new norms will rule the future tiltrotors. In 2014, Leonardo won $380 millions to develop a "Next Generation TiltRotor" design for the offshore market.

Thesis purpose and structure

The presence of the rotor set at the wing tips generates higher vibratory levels than conventional aircraft. Moreover, the maximum speed when operating in airplane mode is limited by *whirl flutter*. It is a dynamic aeroelastic stability phenomenon that may occur in a flexible mounted engine and propeller system. It takes into account the influence of rotating masses, such as the propeller; rotating masses produce additional forces and moments (centrifugal, Coriolis, gyroscopic moments). The fundamental problem is a not symmetrical distribution of lift force on the transversely vibrating propeller. Whirl flutter may cause the propeller mounting to have unstable vibration or even a failure of the engine or a failure of the whole wing.

Whirl flutter

Whirl flutter is a phenomenon that occurs at high inflow conditions, like during high speed cruise flights. It was first identified as dynamic stability problem of propellers around 1938, when relatively massive piston engines were used to power relatively little propellers. In the 1960, after some turboprop crashes, this phenomenon was "rediscovered". The basic study can be done using a simple rotor-pylon system shown in figure 5. The pylon is
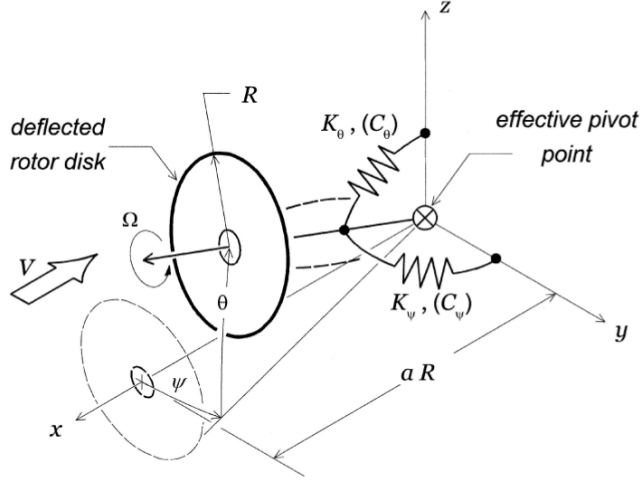
Figura 5: Rotor-Pylon dynamic system (from [5])

pivoted at one point, two rotational springs are used to represent the wing flexibility. The spin axis is oriented in the direction of the flight velocity. The angular perturbations of this vector are θ in pitch and ψ in yaw.

The basic equations of motion for the system are[1]:

$$
\begin{cases}
I_n\ddot{\theta} + C_\theta\dot{\theta} + K_\theta\theta - I_x\Omega\dot{\psi} &= M_\theta \\
I_x\Omega\dot{\theta} + I_n\ddot{\psi} + C_\psi\dot{\psi} - K_\psi\psi &= M_\psi
\end{cases}
\tag{1}
$$

where I_n is the pylon angular moment of inertia (including the diametral moment of inertia of the rotor and nacelle inertia) about the pivot point and I_x the polar moment of inertia of the rotor, $K_{(.)}$ and $C_{(.)}$ are, namely, the stiffness and the damping of the respective degrees of freedom. While M_θ and M_ψ are the applied moments in pitch and yaw, taken about the pivot point, arising from the aerodynamic loads. Using strip theory and quasi-steady assumptions to formulate the perturbational aerodynamic loads yields to the definition of the pitch and yaw moment[2]:

$$
\begin{aligned}
M_\theta &= \frac{b}{2}K_aR\left[-\left(A_3 + a^2A_1\right)\frac{\dot{\theta}}{\Omega} - A_2'\psi + aA_1'\theta\right] \\
M_\psi &= \frac{b}{2}K_aR\left[-\left(A_3 + a^2A_1\right)\frac{\dot{\psi}}{\Omega} + A_2'\theta + aA_1'\psi\right]
\end{aligned}
\tag{2}
$$

---

[1]The symbols are kept equal to the reference [5]

[2]Only results are provided here, for more details see [5]

4

where the coefficients are

$$K_a = \frac{1}{2}\rho C_{l,\alpha} R^4 \Omega^2 \qquad\qquad J = \frac{\pi V}{\Omega R}$$

$$A_1 = \int_0^1 \frac{c}{R} \frac{(J/\pi)^2}{\sqrt{(J/\pi)^2 + \eta^2}} d\eta \qquad\qquad A_1' = \frac{J}{\pi} A_1$$

$$A_2 = \int_0^1 \frac{c}{R} \frac{(J/\pi)\eta^2}{\sqrt{(J/\pi)^2 + \eta^2}} d\eta \qquad\qquad A_2' = \frac{J}{\pi} A_2$$

$$A_3 = \int_0^1 \frac{c}{R} \frac{\eta^4}{\sqrt{(J/\pi)^2 + \eta^2}} d\eta \qquad\qquad A_3' = \frac{J}{\pi} A_3$$

and η is the non-dimensional coordinate that spans the blade. As other aeroelastic instabilities, the addiction of the aerodynamic forces can lead to negative damping. The stability characteristics of the system are functions of several parameters:

- rotor speed Ω;

- polar moment of inertia I_x;

- pylon (nacelle) inertia I_n;

- stiffnesses in the two directions K_ψ and K_θ;

- dampings in the two directions C_ψ and C_θ;

- pivot to hub distance over rotor radius a.

The flutter instabilities are directly related to the gyroscopic precession movements of the rotor; two modes can be seen: forward whirl and backward whirl, see figure 6. The two possible movements are uncoupled if the rotor is not in rotation. The rotation of the rotor couples the two movements in two modes which are stable without the aerodynamic forces.

For the rigid blade rotor considered here, the only flutter instability that can experience comes from the backward-whirl mode; the aerodynamic loads are the drivers for this instability. The qualitative indication of how the stability characteristics of the system depends on the parameters can be found in figure 7. The whirl flutter boundary is extended along the diagonal $K_\theta = K_\psi$, which means that if the two stiffnesses are similar, the system is more prone to flutter than if one of the stiffnesses is reduced. Increasing the pitch damping of the system has a relevant effect on the system. A limited increase of pitch damping can largely reduce the unstable region. Instead, a little increase of the distance between the pivot point and the hub has a limited effect on the unstable region.
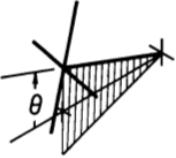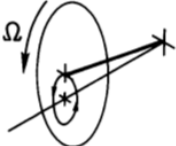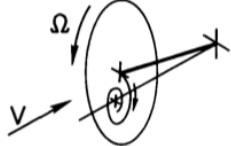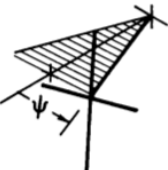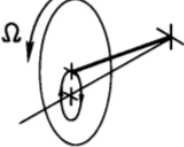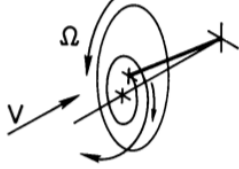
NONROTATING PROP.	ROTATING PROP. WITHOUT AIR FORCES	TRANSIENT RESPONSE WITH AIR FORCES
PITCH	FORWARD WHIRL	STABLE ($V < V_{CRIT.}$)
YAW	BACKWARD WHIRL	UNSTABLE ($V > V_{CRIT.}$)

Figura 6: Whirl modes (from [34])

For conditions of backward whirl, θ and $\dot{\psi}$ are in phase with each other, and ψ and $\dot{\theta}$ are out of phase; these terms act as negative dampers, leading to the flutter instabilities.

The previous analysis is related to a rigid rotor attached to a fixed pivot point, in the reality, however, the pylon is connected to the wing which has its modes and aerodynamics. When the lowest mode of the wing (typically associated with out of plane bending) is close to the whirl flutter frequency, there is an increase of damping, increasing the region of stability. Introducing the elasticity of the blade does not change the phenomenon at the base of whirl flutter, although also forward whirl flutter could happen.

Stability augmentation methods and present work

Because this instability can damage the aircraft, different types of modifications have been studied in the past. Most of them based on active control; Singh *et al.* investigated stability augmentation system of a model of the XV-15 experimental tiltrotor based on Linear Quadratic Regulator (LQR), [29]; Mattaboni *et al.* used a Generalized Predictive Controller (GPC) to control the aeroelastic response of a multibody model of the Wing-Rotor Aeroelastic Testing System (WRATS), [26].

Since whirl flutter is a problematic instability, the aircraft flight envelope has to be free of it, and a passive stability augmentation system is preferable. The increase of speed at which the whirl flutter occurs is the key for a
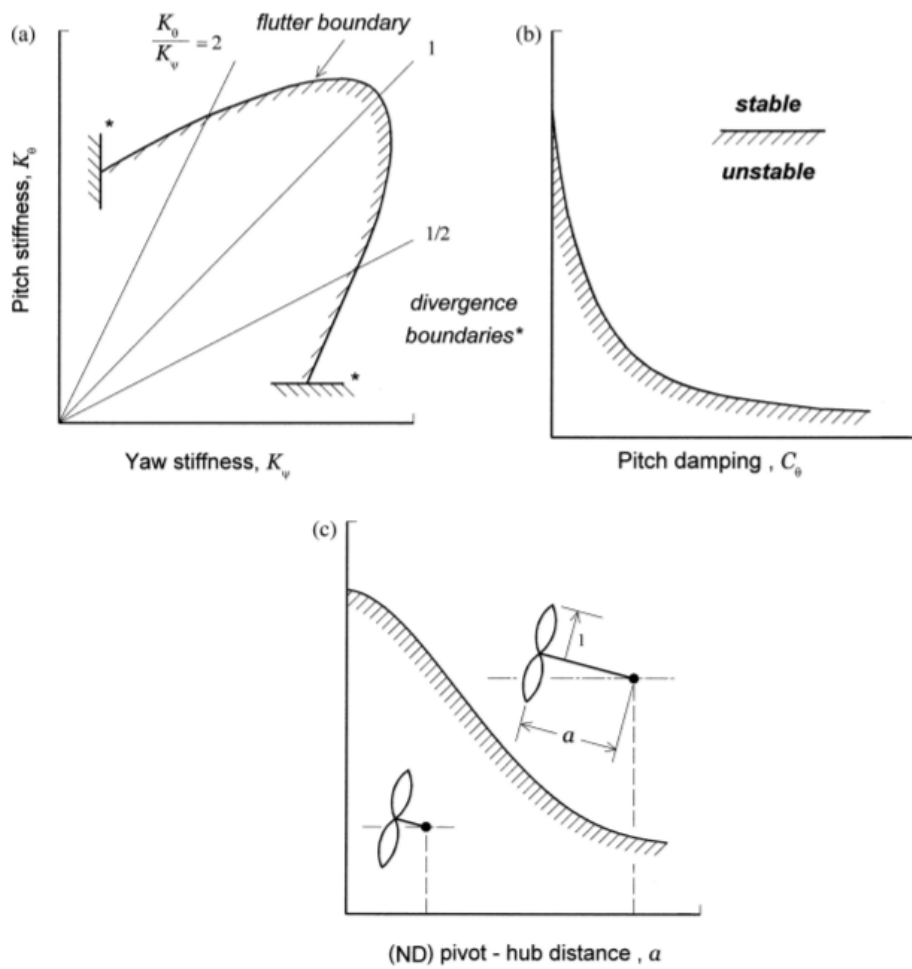
Figura 7: Rotor whirl trends of propeller with rigid blades (from [5])
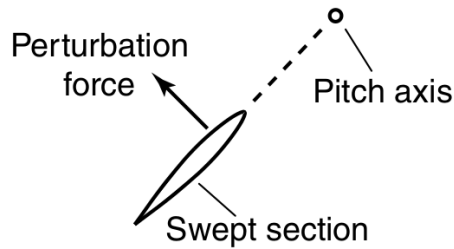
Figura 8: Perturbation force on a swept section (from [7])

successful certifiable aircraft. In the past, the solution was to increase the stiffness and the thickness of the wing. These modifications lead to two penalizing effects, the increase of weight and the rise of drag, limiting the flight envelope of the aircraft. For this reason, during the years different passive methods have been studied, from the use of composite materials to elastically couple the modes of the wing/blade system ([3], [27] and [14]) to the blade geometry design, see [1], [2] and [7]. The blade modifications are focused on the addiction of swept tips. It has been proven that these modifications lead to a higher whirl flutter speeds ([2]) for swept back tips. In classical flutter theory, the distance between the elastic axis and the aerodynamic center is a key parameter. This suggests that a similar fashion is useful for whirl flutter problems. A simple approach can be used to understand the dynamic response of the system. Considering perturbation forces, it is possible to visualize the effect of blade with swept tips on the pitch axis, see figure 8.

The center of pressure moved aft of the pitch axis thanks to the swept tip creates a favorable (nose-down) moment from the perturbation lift. This pitching moment has a stabilizing effect for the whirl flutter because counteracts the increase of force due to coupling of flap and the modes of the wing. A forward displacement of the local aerodynamics center has negative effect on the damping.

This peculiar behaviour is the result of the torsional elasticity of the rotor-blade system. Indeed , using a rotor with rigid blades and rigid pitch link, the application of swept blades has not large effects on the whirl flutter speed. Instead, using flexible blades, the increment of velocity is significant. A more detailed analysis can be found in section 3.1.

The present work aims to find aerodynamic modifications to improve the stability characteristic of tiltrotors to whirl flutter. Several changes are studied: blades with swept tips, blades with double sweep, and gurney flaps. The first modification used, the blade with swept tip, is based on the studies done in [1] and [7]. The double swept blade as been proven to be effective from the performance point of view ([8]); it increases the performances in

hover, modifying the blade vortex interaction, and reducing the tip losses due to the compressibility during high speed flights. However, an aeroelastic study of the problem has not been done yet, so it is provided here. In order to understand the effects of the swept and double swept blades, some parametric studies have been done and discussed in this work.

Moreover, the reasoning done in [7], summarized in figure 8, suggests that increasing the pitching moment of the airfoil section could help to shift the whirl flutter boundaries toward higher limits. To do so, gurney flaps have been chosen. A gurney flap is a small tab installed on the trailing edge on the pressure side of the airfoil; they are also capable of moving the aerodynamic center in direction of the trailing edge of the airfoil equipped with. The aerodynamic modelling of gurney flaps is studied in this work. The derivation of the model comes from a previous work, [32], and an extension is studied here to model the drag. A parametric study of the application of gurney has been done and discussed.

A detailed analysis of the effects of the variations on the tiltrotor system has been done. The extreme cases are compared to the baseline model to understand the effects of adding a swept tip or the gurney flaps to improve the aeroelastic stability of the system. The results are reported in section 3.5.

In order to assess the characteristics of the phenomenon a multibody semi-model of a tiltrotor is used. Due to the fact that the phenomenon is non-linear, an optimisation based on a genetic algorithm has been set up.

The present work is organized as follows. In chapter 1 is described the multibody model used and the analysis of the baseline tiltrotor is discussed. The method to assess the aeroelastic stability of the system is presented in the chapter as well. The chapter 2 describes the gurney flap and its effects on the two dimensional blade section. A method to calculate the coefficients is studied and provided. The effects on the tiltrotor are presented in the chapter as well; the thrust, torque and loads modifications are shown. The following chapter 3 shows the parametric studies done on the simple and double swept blade. The effects of a blade with anhedral angle at the tip are also studied. The aeroelastic reactions of the model to the modifications are shown. A comparison to understand in detail the causes of the augmented stability and the pros and cons of the swept blade and gurney flaps is reported in the chapter. In chapter 4 the optimisation process is explained in detail and the results are shown. The optimal blade is compared with other important design found in this work. At the end, the obtained results are briefly summirized and future developments are presented in chapter 5 of the thesis.

Capitolo 1

Tiltrotor model

In the present work, a multibody model for MBDyn (see A) has been used for the numerical simulation of the tiltrotor. The model has been inspired by NASA's WRATS model. The acronym WRATS stands for Wing and Rotor Aeroelastic System that is a semi-span aeroelastic wind-tunnel model tested at the TDT (Transonic Dynamic Tunnel) of NASA's Langley Research Center (LaRC). It was developed to support the preliminary design and the development of the tiltrotor Bell Boing V22-Osprey, successor of the Bell XV-15. The model is a multibody representation based on the real system implemented in MBDyn, see [10]. The version used in the present work has been similar to the original version of the WRATS with a three-blade hingeless stiff-inplane rotor.

The chapter is divided in three sections. In the first one, the multibody model is briefly described focusing on the elements used. In the second section, the analysis of baseline model is provided and the choices done are explained. In the last section, the conditions chosen to assess the whirl flutter response of the system are described.

1.1 Model description

The multibody model in MBDyn has been developed following the data that can be found in [28]. Some variations have introduced following the work done in [25], the stiffnesses of the wing have been reduced and the blade stagger has been increment of 20°. The main geometry characteristics can be found in table 1.1.

The model consists in different parts assembled together and analysed as a whole. These parts are the following:

wing: it is modelled using six beam elements at three-node that use a finite element approach described in [9]. Wing aerodynamics is modelled using a quasi-steady strip theory with lookup tables for the aerodynamic coefficients. The six beams are attached to as much aerodynamic

Parameter	Value (UCSU)	Value (SI)
wing mass	0.74 slugs	10.80 kg
pylon mass	1.28 slugs	18.68 kg
rotor mass	0.43 slugs	6.27 kg
total mass	2.45 slugs	35.75 kg
wing span	3.45 ft	1.05
wing chord	2.1 ft	0.64 m
number of blades	3	
rotor radius	3.8 ft	1.16 m
rotor solidity σ	0.0965	
rotor speed Ω - airplane mode	742 rpm	77.70 rad/s
rotor speed Ω - helicopter mode	888 rpm	92.99 rad/s

Tabella 1.1: Tiltrotor model: principal dimensions and masses

panels, which in MBDyn implements a quasi-steady strip theory, see B for more details.

pylon: this element permits the rotation of the rotor from helicopter to airplane mode and vice versa. It is attached to the wing tip at one extremity and to the mast at the other one. It can tilt with respect to the wing tip. It is modelled as a joint with mass and inertia properties.

mast: it is modelled using two two-node beam elements. The mast has an imposed rotation given by an axial joint that permits one node to rotate along an axis with respect to another one. Three bodies have been used to add mass and inertia properties.

swashplate: it is modelled on a physical basis that replicates the exact kinematics of the blade pitching mechanism. It consists of two rigid bodies joined by a plane hinge that depict the two plates. The fixed plate is linked through an in-line joint (the nodes are constrained to move on the same line) to the pylon, the rotating plate can rotate with respect to the fixed one at the velocity imposed by the axial joint on the mast. A total joint is used to control the collective pitch, fixing all the unnecessary movements and governing the movement aligned with the mast. A rod with offset is used to simulated the control chain flexibility.

rotor: it is implemented using an ideal gimbal joint, see [23], that connects the hub and the mast. This particular joint allows two nodes to rotate one respect to the other keeping fixed the angular velocity with respect to two arbitrary axes.

blades: two different models are available, one rigid and one flexible, both share the same mass, inertia and aerodynamic properties and the flexbeam
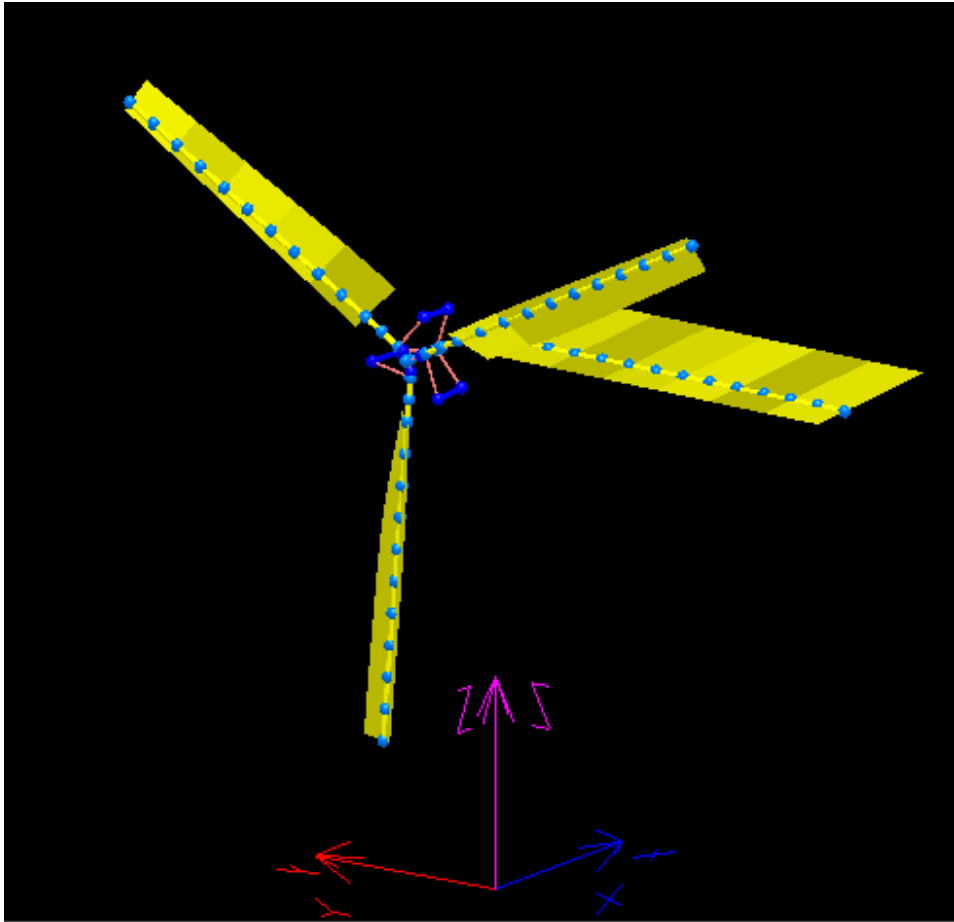
Figura 1.1: Representation of the MBDyn tiltrotor model using EasyAnim

element. To model the latter is used a three-node beam element. The link between the blade and the flexbeam relied on a gimbal joint plus an in-line joint. Whereas a distance joint models the control link connecting the rotating swashplate and an offset point aft of blade cuff. The flexible blade uses five three-node beam elements. The rigid blade is modelled as a rigid body. Like the wing, the blades are attached to five aerodynamic panels.

A representation of the MBDyn model can be found in figure 1.1 and 1.2. The highly twisted blade is well visible. The wall at which the wing is attached is not represented, however, the tip of the wing without the rotor is constrained to a fixed point.
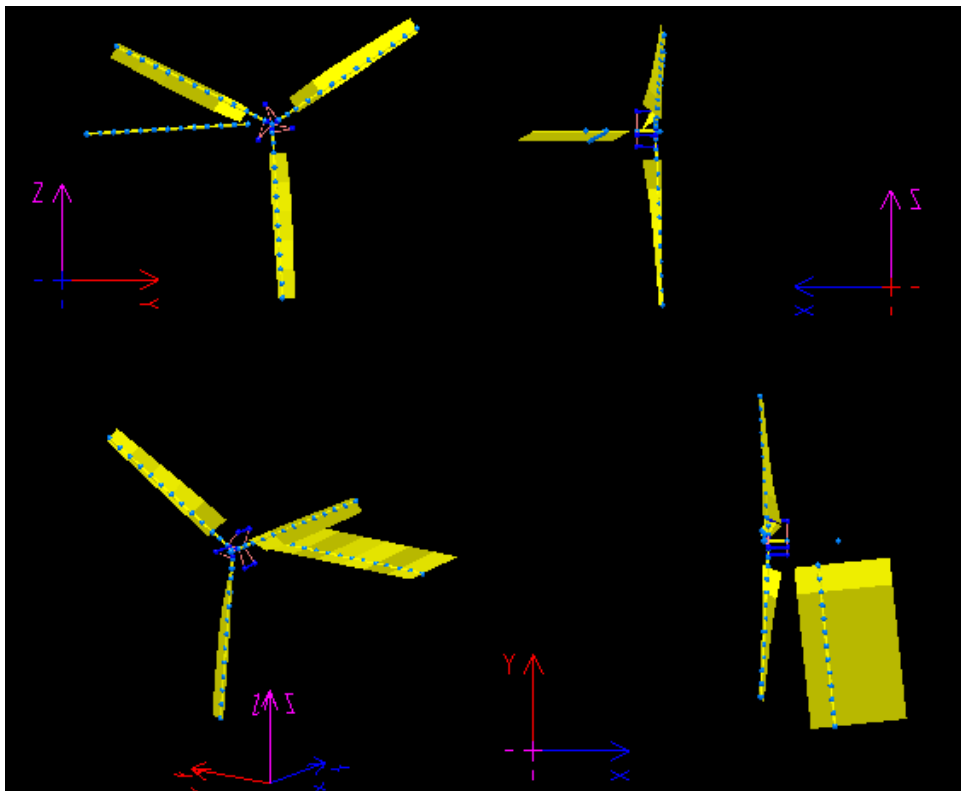
Figura 1.2: Orthographic projections of the MBDyn model using EasyAnim
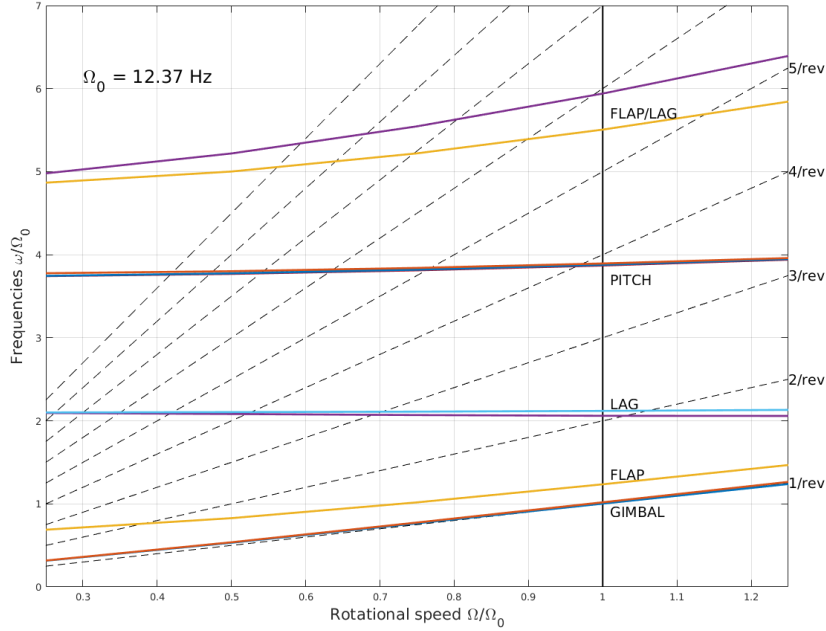
Figura 1.3: Fan plot of the isolated rigid rotor in vacuo

1.2   Baseline configuration analysis

The model definition is always an iterative process. Several attempts have been done to reach an acceptably approximation of the system. In this process, some variation has been added and tested. First, a rigid rotor without torsional stiffness has been used. However, the results were discording with respect to the ones in [1], see 3.1. Then a flexible pitch link has been used to take into account the flexibility of the control chain. More suitable results have been found. The final step was the introduction of flexible blades.

The rotor isolated has been studied in order to check the rotor frequencies. A model with rigid blade has been used to keep the simulation simple because the main frequencies are substantially not affected by the introduction of elastic blades. The rotor is equipped with rigid blades and a flexible pitch link to provide the first torsional frequency at around 3.8/rev. The fan plot of the rigid rotor in vacuo is shown in figure 1.3. Differently from helicopter applications, the rotor of tiltrotors requires a large variation of collective pitch to compensate the largely variable inflow speeds. Moreover, the blades of tiltrotor are usually highly twisted to have good performances during cruise, i.e. the blade used here has 35° of twist. For these reasons, the main rotors frequencies are more dependent on the pitch angle with re-

15

spect to helicopter's blades. A collective angle expected at 135 kts has been used to study the rotor frequencies[1].

The rotor is a stiff-inplane three-blade gimballed rotor. In this kind of rotors, the blades are attached to the hub without flap or lag hinges, and the rotor is attached to the mast by a gimbal joint, ideally cancelling the transmission of moments to the mast. The hub has two possible movements, the longitudinal and lateral rotations which correspond to the tip-path-plane tilt of an articulated rotor by cyclic flapping. In the present work, these two motions are called "gimbal" modes. The gimbal modes can be restrained using springs, indeed, the frequencies of these modes are at 1/rev, and the springs are used to slightly move the modes above the 1/rev. This behaviour is well visible in figure 1.3. The coning motion of the blades behaves as on a hingeless rotor, and also for higher harmonics the hub remains fixed. The rotor has a negative δ_3 angle of 15°, creating a negative pitch-flap coupling (flap up causes pitch up). The negative pitch-flap coupling is used on gimballed rotors to avoid flap-lag aeroelastic instabilities. Like teetering rotors, gimballed ones are usually stiff-inplane to avoid a mechanical instability called ground resonance and other aeroelastic instabilities, see [13]. Indeed, the lag frequency is above 1/rev. The rotor is equipped with a 2.5° precone angle to reduce the loads both in airplane and hover conditions.

The present work is focused on the stability during high speed flights. In order to reduce the simulation time, and consequently the optimisation time, an uniform inflow model has been used, as done in [7]. The use of this simple model is adequate for whirl flutter analyses. The direction of the airflow is usually parallel to the mast and the tip losses are small compared to the helicopter mode. A more sophisticated model than the uniform inflow is unnecessary.

The aerodynamic model is a quasi-steady strip theory implemented in MBDyn, the stall is taken into account only through the lookup tables of the sectional airfoils, see appendix B. The quasi-steady assumption is justified by previous work ([15]) where using an unsteady aerodynamics results in an increase of whirl flutter speed. Moreover, the complexity of the model is lower and the computational cost decreases.

The airfoils used are NACA 0012 that are able to give good results studying the stability of tiltrotors, see [24].

The isolated rigid rotor model has been tested in axial flow up to 250 kts and no instabilities arisen. For this reason, it has been safe to use this rotor on a tiltrotor model that can exceed the baseline whirl flutter velocity.

The rigid blade rotor has been introduced on the tiltrotor model. Some tests on the aeroelastic characteristics have been performed. In a similar way of [2], the blade panel position has been modified trying to reproduce the results. The mass properties of the blade have been kept fixed to maintain a

---

[1]The explanation of the speed chosen will be provided in next chapters.

MBDyn elements	number of elements
structural node	45
body	91
beam2	14
beam3	21
aerodynamic beam3	21
joint	47

Tabella 1.2: Tiltrotor MBDyn model summary

simplified model. Unfortunately, the rigid rotor has not been able to reach the enhancements illustrated by Acree.

Then a rotor with flexible blades has been used in the tiltrotor model. As expected, the introduction of the flexible blades with swept tips extends the whirl flutter velocities. A more detailed description is provide in chapter 3.

A summury of the MBDyn elements of the model can be seen in table 1.2. The total number of degrees of freedom is 387. MBDyn uses a state space form, accordingly the number of equations to be solved are 774. In order to have the dimensions of the system, it is necessary to add the number of constraint equations, that is 53, so the system is composed by 827 equations (see appendix A for more details).

In order to estimate the correct number of strips to be used, a parametric study has been done. A rotor with flexible pitch link and flexible blades has been used. The variation on the response of the system due to the change in the strips' number has been done using a swept blade. The use of swept blades is the worst basic case that the model encounters in this work, for this reason, it has been chosen to validate the aerodynamic model. Two different sweep angles have been used. The definition of the angles is in figure 1.4.
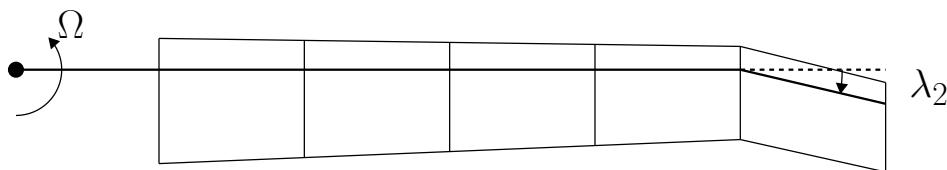
Figura 1.4: Simple swept blade example

The conditions chosen are at the whirl flutter speed, indeed, the scope of the work is to increase it. Potentially differences at this speed are clearly counterproductive. The thrust has been kept fixed at $50 lbf$ as explained lately in 1.2.1. The results are summarised in table 1.3 and table 1.4.

The effects are minor; only slightly changes in the torque values are present. The number of strips has been kept equal to 2 because there is no

$\lambda_2 = 15°$		
Number of strips	2	5
Whirl flutter velocity $[kts]$	169	169
Torque $[lbf\ ft]$	205	206
$\Delta\theta_0$ $[°]$	1.25	1.25

Tabella 1.3: Summary of the parametric analysis on the number of strips for $\lambda_2 = 15°$

$\lambda_2 = 25°$		
Number of strips	2	5
Whirl flutter velocity $[kts]$	180	180
Torque $[lbf\ ft]$	229	231
$\Delta\theta_0$ $[°]$	1.9	1.9

Tabella 1.4: Summary of the parametric analysis on the number of strips for $\lambda_2 = 25°$

reason to increase it.

1.2.1 Whirl flutter

In order to understand the aeroelastic response of the system, the analysis of the baseline model has been performed. Looking forward to the optimisation, also the definition of the parameters for it has been defined in this part of the work.

The stability analysis of complex systems can not be easily done. If the equations of motion of the system can be cast in the form of linear, ordinary differential equations with constant coefficients, classical stability analysis methodologies can be used. In tiltrotors, the presence of the rotors introduces non-linearities in the governing equations that makes impossible the use of analytical methods without introducing further approximations.

Some tools are available for stability analysis, such as Lyapunov direct method, characteristic exponent method and Prony's method, see [4], however they are complex and time consuming. Indeed, they usually requires the use of multiple responses of the system, for this reason the use of these methods during the optimisation is unthinkable.

A simpler approach has been used in the present work, the response of the simulation has been analysed in the time domain to assess the stability of the system to whirl flutter. In order to assess the aeroelastic stability, the model has to be trimmed in a steady state condition, then, the response to a perturbation force can be studied. Three key points can be identified in this process: trim of the model, a force to perturb the system and the stability assessment. All the parameters of these three points have been identified on the baseline model.

(a) Thrust   (b) Torque
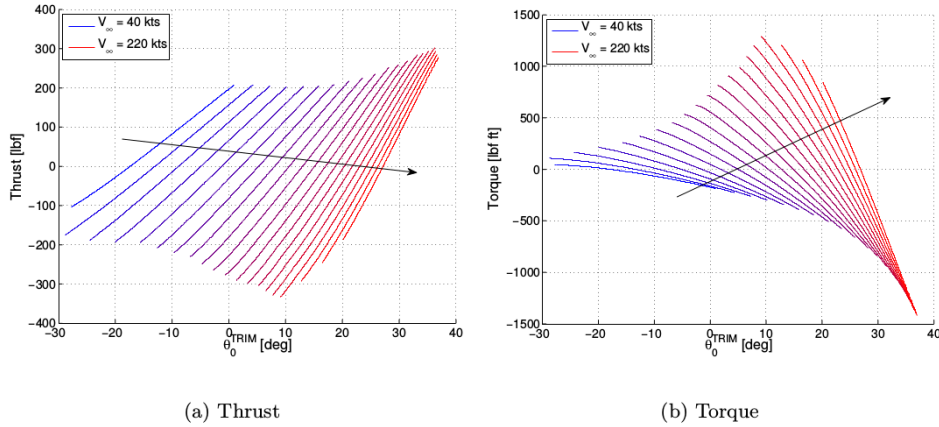
Figura 1.5: Isolated rotor performances(from [25, p.82])

To trim the model in a steady state condition, the corrects value of collective pitch have to set in order to provide the right amount of thrust/power. The work done by Mattaboni in [25] has furnished a excellent starting point, the thrust and torque curves have been used as basis and an increment of the collective pitch has been added to counteract the effects of the new rotor geometry and stiffnesses.

The basis collective-thrust (a) and collective-torque (b) curves for different asymptotic speeds are shown in figure 1.5. Fixing the velocity, increasing the collective pitch increases almost linearly the thrust. A similar behavior is expected in the present work, indeed the major differences are in the flexibility of the control chain. This modification moves the curve slight toward higher pitch angles. The increase of thrust needs major collective angle, consequently the slopes of the curves are expected to be lower. These effects are transmitted also to the torque; the curves move toward higher angles, and the slope is expected to be higher.

Different trim conditions can be considered for aeroelastic calculations:

- constant thrust;

- windmill.

The first one is the most realistic situation: during cruise flight, the rotor-engine group is set on a regime to provide the right amount of thrust to counterbalance the drag. Instead, the windmill condition, in other words zero torque condition, for some tiltrotors is the conservative choice. The windmill corresponds to a possible emergency flight condition (engine out). On the baseline model both the conditions have been studied to choose the most conservative one for the optimisation. Following the idea in [25], the thrust has been set at $50\,lbf$ for the constant thrust trim condition.

19

Then the parameter of the perturbation force have been selected using the baseline model. The parameters include the time history, the application position and the magnitude. They are also constrained by the use of the force for the optimisation procedure. In general, long time histories have to be avoided because the use of a genetic algorithm. The use of frequency sweep over all the possible frequencies of the system is unthinkable. A possible frequency sweep around the modes that have been expected to become unstable has been tested. The modes are the firsts of the wing [2] (see [1], [7] and [25]). However, the result has been the same of a impulsive force but more time consuming. For this reason, after several attempts, an impulsive force has been chosen. In table 1.5 the parameters of the force used are summarized. An impulsive force (doublet) as two successive steps has conducted to unstable calculations, a rounded impulse (doublet) is used instead, see figure 1.6.
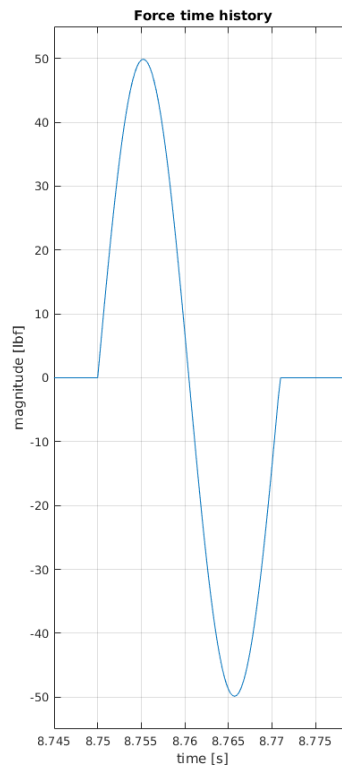
Figura 1.6: Force time history

[2]The system is non-linear and the modes can not be simply decoupled or associated with only a part of the structure.

20

Parameter	Value
Amplitude	$50\,lbf$
Impulse duration	$12\,ms$
Position	wing tip

Tabella 1.5: Exiting force parameters

As well as the other parameters, the application point has been selected after several attempts. It has been proven that the application of the force at the wing tip is capable of excite the modes that become unstable. The magnitude of the force has been chosen to introduce enough energy into the system.

Usually the dynamic deformation associated to the wing modes is more visible at the wing tip. The out-of-plane, in-plane and torsional displacements have been monitored. During whirl flutter, the movements that experience high oscillation are the out-of-plane the in-plane ones.

After several attempts, a doublet on the wing tip has been chosen. It has permitted to excite the modes related to the whirl flutter for the model which are the out-of-plane and in-plane bending.

In order to check the stability of the system, the displacements at the wing tip have been monitored as well as the blade tip displacement with respect to the rotor disc. To define a value that can be related to the damping of the system, an exponential function has been fitted on every displacement:

$$f_i(d_i) = A_i e^{\xi_i} \tag{1.1}$$

where the amplitude A_i and the exponent ξ_i depend on the movement selected.

The exponent can be related to the damping of the system. The idea is that the increase of the exponent can be related to the increase of damping of the corresponding displacements. This method is similar to the "logarithmic decrement method", capable of evaluate the damping of a single degree of freedom underdamped system. The method is simple and effective and it is also simple to implement. These characteristics are perfect in the context of optimisation.

An example of stable wing displacements is reported in figure 1.7. All the movements decays after a certain period of time. The velocity of the decay can be related to the damping of the system.

An example of the fitted exponential function used to evaluate the damping is visible in figure 1.8.

Instead, a unstable displacement example is shown in figure 1.9. The displacement is subject to increasing amplitude oscillations.

Both the trim conditions, fixed thrust and windmill, have been tested and the results are reported in table 1.6.
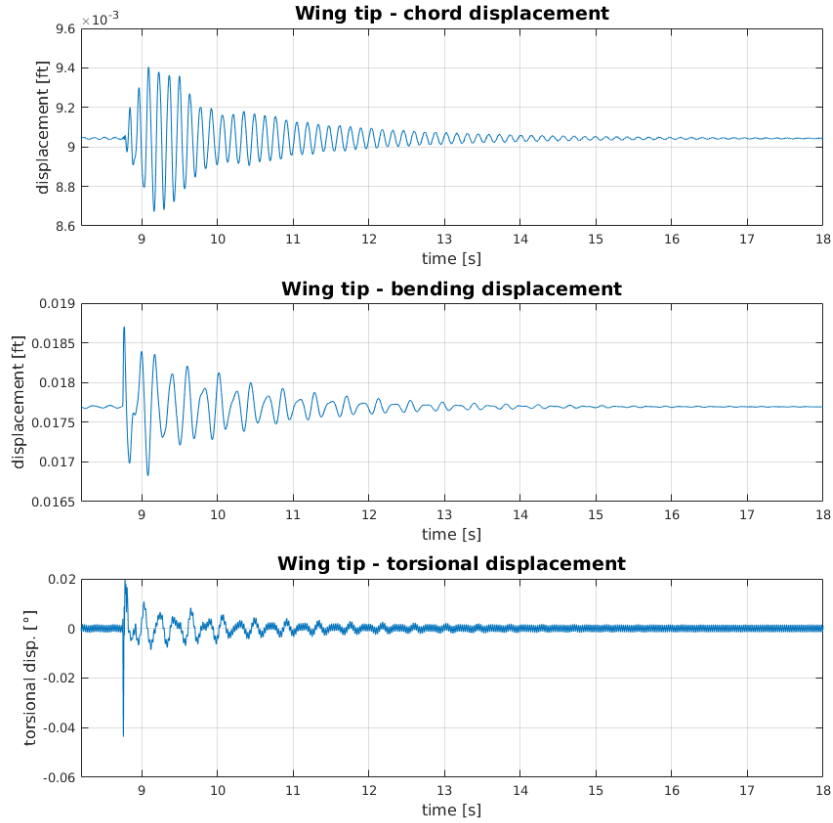
Figura 1.7: Example of stable movements

For the tiltrotor model studied here-in, the whirl flutter speed at constant thrust is lower than the windmill condition. Also the difference is quite high, however, usually the thrust of the system is limited by the power available, and in the present work, no limitations have been set on it.

It is important to notice the small difference in the collective pitch angle. The high inflow is responsible for it; modifying of a small amount the collective pitch is capable of generates large thrust/torque variations.

In order to be conservative in the optimisation process, the constant thrust trim has been used which is the worst condition for this particular tiltrotor configuration.

The difference between the two trim conditions is also related to the amount of thrust selected. Indeed the whirl flutter speed decreased as the increase of thrust, as visible in figure 1.10.
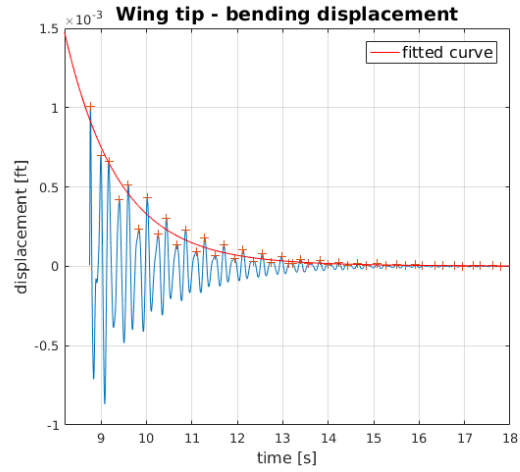
Figura 1.8: Example of exponential fitting on the bending movement

	Fixed thrust	Windmill
Thrust	$50\,lbf$	$-6\,lbf\,ft$
Torque	$162\,lbf$	$0\,lbf\,ft$
Whirl flutter speed	$149\,kts$	$165\,kts$
Collective pitch angle	$29.18\,^\circ$	$31.95\,^\circ$

Tabella 1.6: Results summary of the baseline tiltrotor model

23
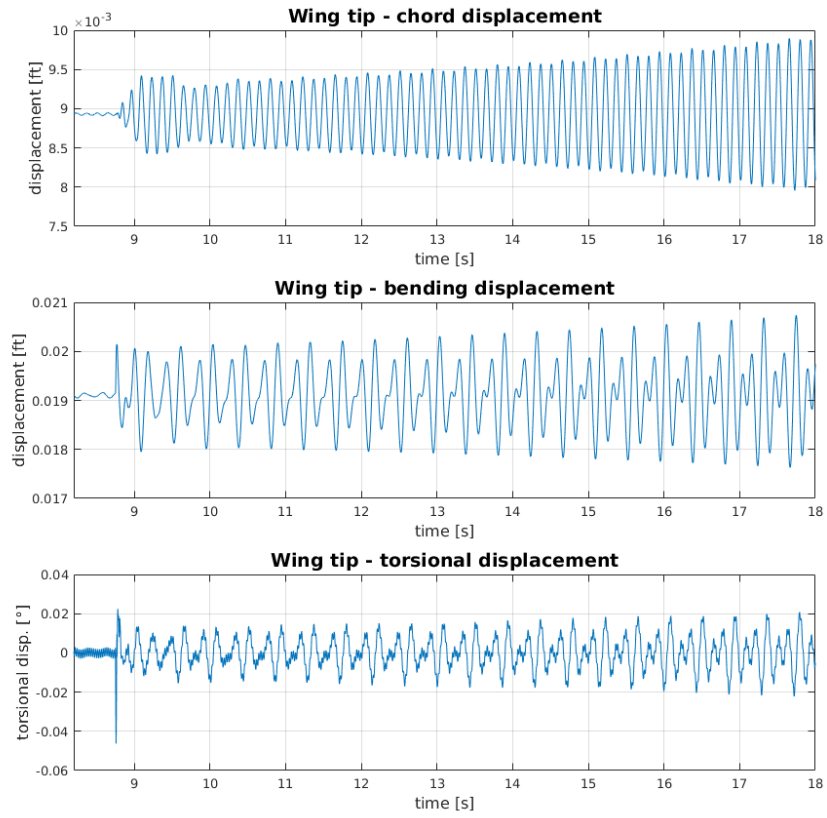
Figura 1.9: Example of unstable movements
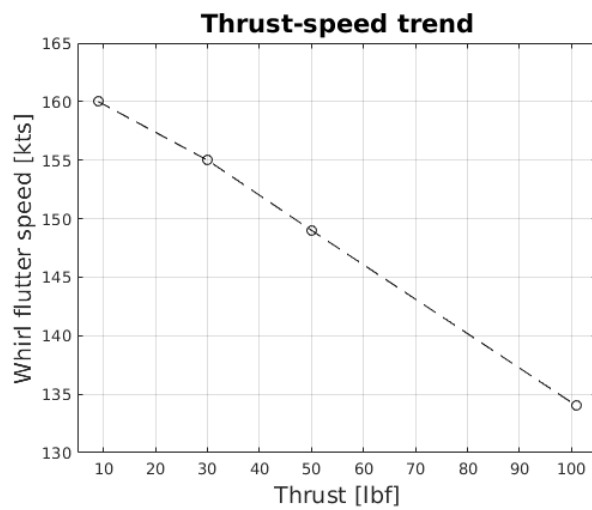
Figura 1.10: Whirl flutter speed function of thrust produced

24

Capitolo 2

Gurney flaps

The gurney flap was developed by Daniel Sexton Gurney in the early 1970s for automotive applications. It is a small tab installed on the trailing edge on the pressure side of the airfoil, normally, perpendicular to the mean chord line. The device allows to modify the Kutta condition and the pressure distribution on the airfoil. The results is a modification of the circulation and so, an increase of lift. The costs of this gain are the increase of drag and aerodynamic pitching moment. There are several studies on the physical mechanism of the gurney flap lift enhancement, see [33] for a complete guide. In the present study, the gurney flap has been used to generates a twist down of the blade and a displacement of the aerodynamic center.

The chapter is composed by three sections. The gurney flaps are described in the first section and the aerodynamic characteristics of the modified airfoil are explained. In the second section, the process to estimate the aerodynamic coefficients is studied in detail trying to explain pro and cons. In the last section, the effects of the application on the tiltrotor model are reported and studied.

2.1 The effects of the gurney flap

The gurney flap is simply a short flat plate attached to the trailing edge, normally, perpendicular to the chord line on the pressure side of the airfoil, it is shown in figure 2.1.

The effects of the gurney are:

- increase of lift with small changes of the stall angle of attack

- increase of drag

- increase of aerodynamic moment at the quarter chord.

The gurney flap modifies the Kutta condition at the trailing edge of the airfoil. Imposing a finite pressure difference at the trailing edge in a panel
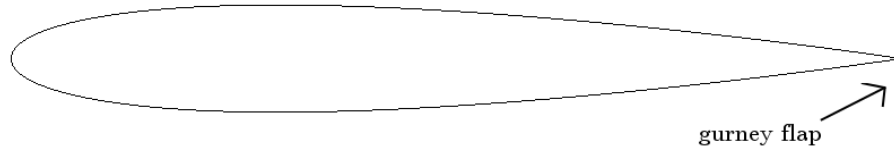
Figura 2.1: NACA 0012 equipped with a 3%c gurney flap
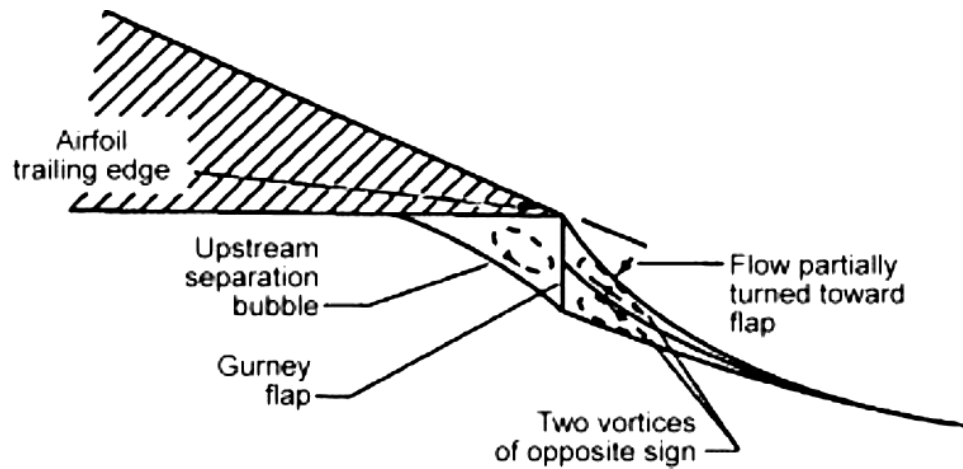
Figura 2.2: Liebeck's hypothetical flowfield about a Gurney flap (from [19])

method is possible to replicate the aforementioned effects, as *Jeffrey et al* did in [12]. Many studies were done in order to understand the mechanism responsible for the lift enhancement of the gurney flap. Only a short explanation will be given here, for further examination see [33].

As touched upon, the Kutta condition is modified by the presence of the gurney. The behavior of the flow depends on the angle of attack and the airfoil shape.

In all cases, there is a recirculation region upstream of the flap on the surface where it is installed, generating an adverse pressure gradient in front of the flap, as shown in figure 2.2. Downstream the flap, the flow field shows a pair of counter-rotating vortices. The latter moves further downstream the rear stagnation point. The presence of these vortices reduces the adverse pressure gradient near the trailing edge, leading in a delay of flow separation. The velocity upstream the gurney flap is reduced, the pressure on the lower surface of the airfoil increases. The overall effect is an increase of the total circulation, so higher lift is produced. Unfortunately, the generation of lift involves a rise in drag. The better way to visualize the drag growth is measuring the wake momentum deficit, visible in figure 2.3.

26
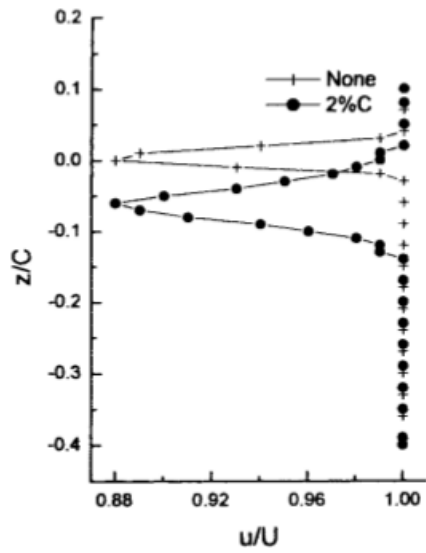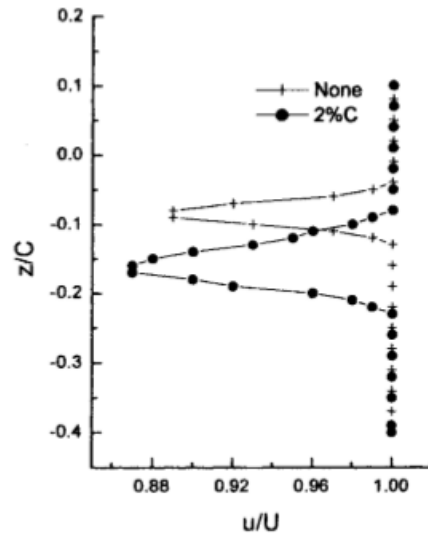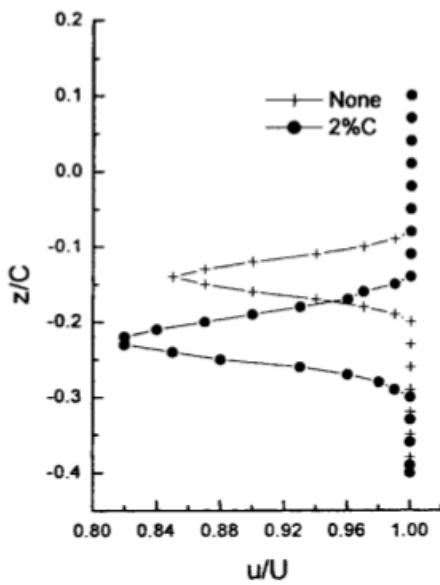
Figura 2.3: Wake velocities profile on NACA 0012 without and with 2%c gurney (from [17])

Several studies show a modification of the wake, the presence of gurney increases and widens the momentum deficit and, accordingly, the drag increases. The visualization of the flow shows a downward shift of the deficit as if the camber has been increased by the gurney flap. This is consistent with a theoretical interpretation that can be found in [20]. Due to the increase of rear load, there is a gain in the moment around the quarter chord. The growth of lift, drag and moment is function of the gurney height and position, the optimum lift-to-drag ratio scales as the boundary layer thickness. The optimum height for the gurney is lower then the boundary layer thickness at the trailing edge ([17] and [35]). An example of the effects on the aerodynamic coefficients can be seen in figures 2.4, 2.5 and 2.6 that show the coefficients of lift, drag and pitching moment[1] of a NACA0012 with several gurney flaps from [17] installed at trailing edge. Instead, the lift to drag ratio is visible in figure 2.7. Data above 12° of angle of attack are not reported because in the present work were unnecessary, moreover, only the clean configuration and the airfoil with a 0.5% flap are not in stall conditions over it. Consequently the stall angle of airfoil with gurneys is slightly lower than in clean configuration and, the lift coefficient curve is shifted upwards. These effects are similar to an increase of curvature of the mean line. Looking at the drag coefficient, it is visible a general increase of drag, and a transfer of the minimum C_D for $h/c = 3\%$. Probably, this particular value is due the high height of the gurney flap, taller than the boundary layer at the trailing edge producing more drag at low angles of attack. Concerning the pitching moment at 25%c, it can be seen a shift downwards with respect to the clean configuration values like the lift coefficient, probably because those are related. The effects on the lift and drag coefficients are also visible on the lift to drag ratio curves.

Unfortunately, the behavior of the flow is very difficult to predict using both analytical and numerical models. In order to find the correct values of coefficients a semi-empirical algorithm has been used.

2.2 Coefficients estimation

Finding the correct values of the aerodynamic coefficients is, up to now, analytically impossible. In the present work, a semi-empirical model, following the work done in [32] and [20], has been used. As noted from different experiments and from *Liu* and *Montefort*'s analysis, [20], the shift of the zero-lift angle of attack is proportional to $\sqrt{h/c}$. For a thin airfoil in clean configuration, up to the stall angle of attack, the lift coefficient can be written as

$$C_L = C_{L,\alpha_{h/c=0}}(\alpha - \alpha_{0_{h/c=0}}). \tag{2.1}$$

---

[1]The pitching moment is referred to the conventional point at 25%c.
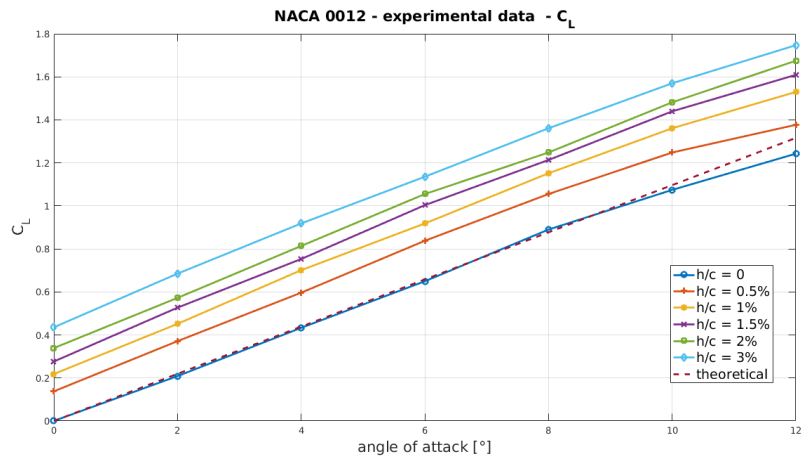
Figura 2.4: Lift coefficient experimental data of NACA0012 equipped with gurney flaps of different sizes from [17]
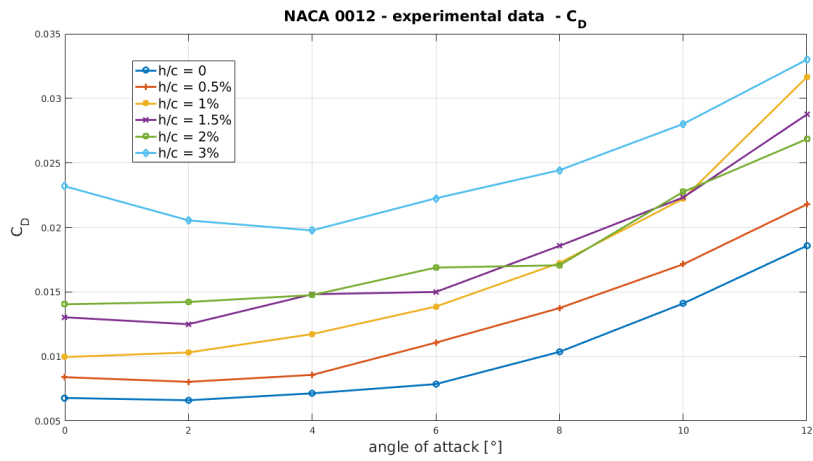
Figura 2.5: Drag coefficient experimental data of NACA0012 equipped with gurney flaps of different sizes from [17]

29
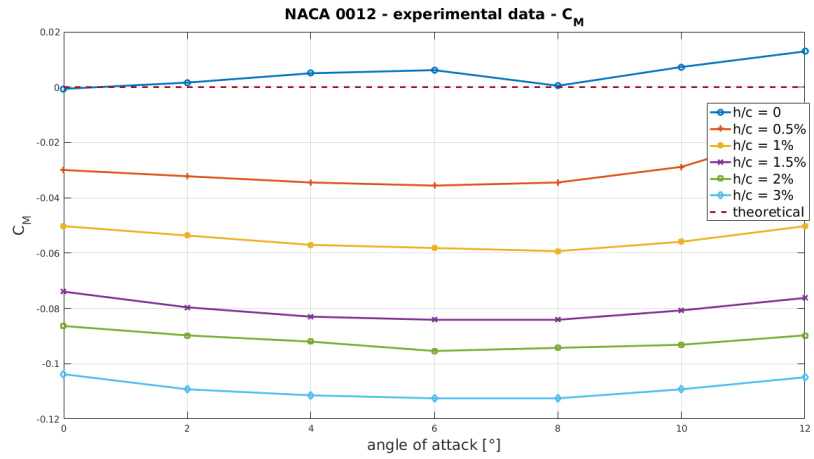
Figura 2.6: Pithing moment coefficient at c/4 experimental data of NACA0012 equipped with gurney flaps of different sizes from [17]
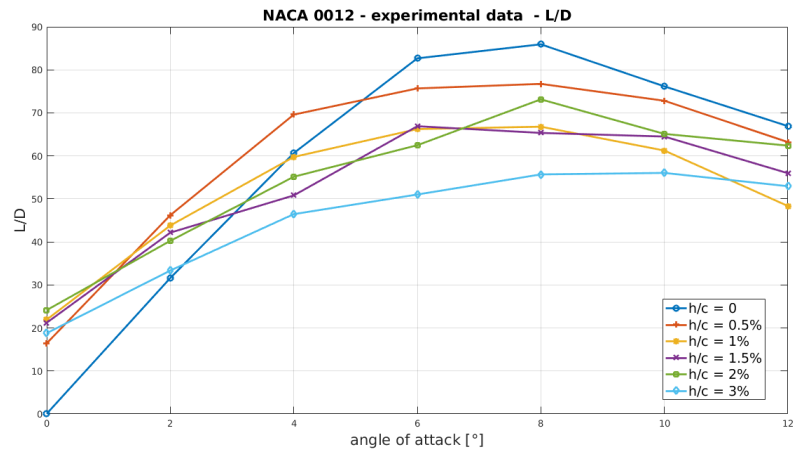
Figura 2.7: Lift to drag ratio experimental data of NACA0012 equipped with gurney flaps of different sizes from [17]
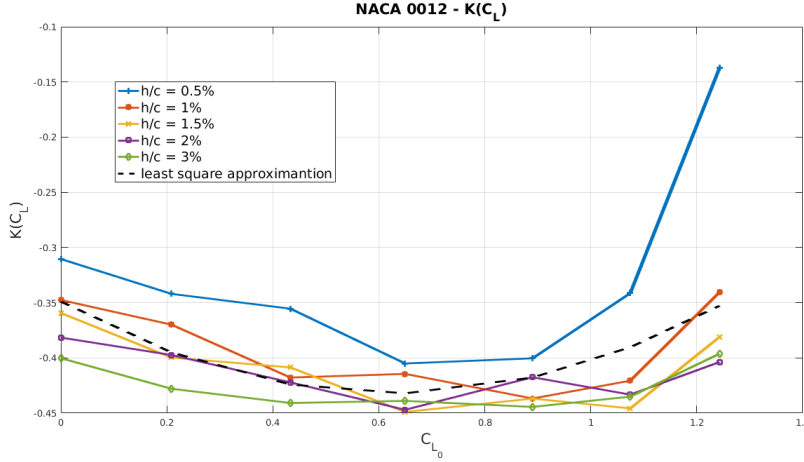
Figura 2.8: Lift corrective coefficient for NACA 0012

When a gurney flap is installed, the formula can be rewritten as

$$C_L = C_{L,\alpha_{h/c=0}}(\alpha - \alpha_{0_{h/c=0}} - K(C_L)\sqrt{h/c}). \qquad (2.2)$$

Solving the equation (2.2) for $K(C_L)$ yields

$$K(C_L) = \frac{\alpha - \alpha_{0_{h/c=0}} - (C_L/C_{L,\alpha_{h/c=0}})}{\sqrt{h/c}}. \qquad (2.3)$$

This coefficient $K(C_L)$ can be found using experimental data. For the current work, they have been used the experimental data in [17], that are referred to a NACA 0012 equipped with different flaps, replied in figures 2.4, 2.5 and 2.6. It has been chosen because the previous work done on a MBDyn tiltrotor model used the same profile with good results for whirl flutter boundaries, see [24]. Moreover, the use of a different airfoil implies a redesign of the entire propulsive system.

The corrective coefficient $K(C_L)$ shows a quadratic trend of the type

$$K(C_{L_{0012}}) = a_2(C_{L_{0012}})^2 + a_1(C_{L_{0012}}) + a_0 \qquad (2.4)$$

with respect to the lift coefficient independent from the flap height as it can be seen in figure 2.8. Theoretically, the trend is also independent from the type of airfoil. It can be seen an interesting behaviour, for relatively high angles of attack, the curve relative to the airfoil equipped with a $0.5\%c$ gurney flap is far from the others. The lift curves of this airfoil are very similar to the clean configuration, indeed, the stall angles of attack are equal. Unfortunately, this behavior significantly affects the model for the corrective coefficient. Also for the previous angle of attack the points act like outliers but they can not be excluded. Moreover, the point at $C_L \approx 0.4$ or
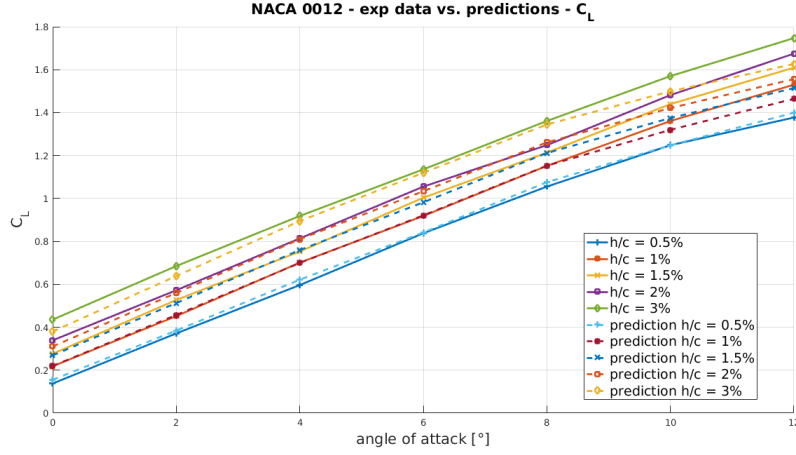
Figura 2.9: Lift coefficient comparison between experimental data and predictions for NACA0012 with gurney flap

$\alpha = 6°$ behaves like an outlier but, due to the low number of measurement, it can not be excluded as well. A comparison between the prediction and experimental data can be found in figure 2.9.

The predictions are quite similar to the experimental data for h/c below $3\%c$ up to $\alpha = 8°$. As previously mentioned, the error is large for high angles of attack due to the "ouliers". However, the model can be considered usable because at whirl flutter conditions the velocity is high and the amount of thrust required can be produced at very low angles of attack of the blades. A study of the conditions on the baseline model has be done near whirl flutter conditions and, the results can be seen in table 2.1. Supposing a similar behaviour for the swept blade, it has been reasonable using the computed model.

The pitching moment coefficient has be found using the link discovered by *Liu* and *Montefort* in [20]. They had found a very simple correlation involving the variation of lift and the variation of pitching moment at the quarter chord, the following

$$\frac{\Delta C_L}{\Delta C_{M_{c/4}}} \approx -4. \tag{2.5}$$

Using (2.2) it simple to find

$$\Delta C_L = -C_{L,\alpha_{h/c=0}} \, K(C_L) \, \sqrt{h/c} \tag{2.6}$$

that represents the increment of lift due to the presence of gurney flap. Defining

$$\Delta C_{M_{c/4}} = C_{M_{c/4}} - C_{M_{c/4,h/c=0}} \tag{2.7}$$

and using (2.6) and (2.5), it yields

$$C_{M_{c/4}} = C_{M_{c/4,h/c=0}} + \frac{1}{4} C_{L,\alpha_{h/c=0}} K(C_L) \sqrt{h/c}. \qquad (2.8)$$

which is a simple relation also for the pitching moment coefficient. The results of the model can be seen in figure 2.10.
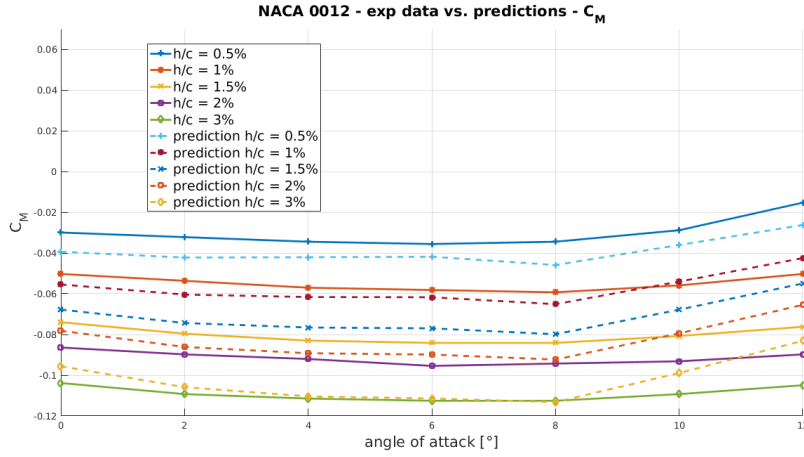
Figura 2.10: Pitching moment coefficient comparison between experimental data and predictions for NACA0012 with gurney flap

There is a good general correlation with the experimental data. A slightly upward displacement is visible except for the smaller flaps. The differences are in general small so the use of this approximation is justified.

Concerning the drag coefficient a similar work has been done. In the previous studies the drag coefficient is not taken into account. In order to use these particular airfoils in the model, a similar method to predict it has been developed. It has been suppose the drag coefficient divisible in two different contributions, one due to the clean configuration and one due only to the presence of the gurney flap. This assumption yields

$$C_D = C_{D_{0012}} + C_{D_G}. \qquad (2.9)$$

Since the presence of gurney modifies the pressure field around the airfoil and drag depends on the flap height, as you can see in figure 2.5, the aerodynamic drag must be a function of the lift coefficient and the flap height,

$$C_{D_G} = Z\left(C_{L_{0012}}, \frac{h}{c}\right). \qquad (2.10)$$

Analysing the available data a simple relation has been found
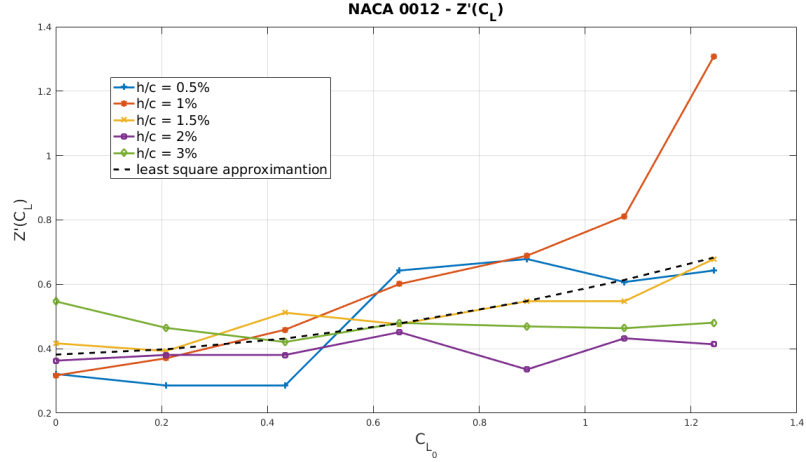
Figura 2.11: Drag corrective coefficient for NACA0012

$$C_{D_G} = \frac{h}{c} Z'(C_{L_{0012}}) \tag{2.11}$$

where $Z'(C_{L_{0012}})$ is a quadratic function

$$Z'(C_{L_{0012}}) = a_2 (C_{L_{0012}})^2 + a_1 (C_{L_{0012}}) + a_0 \tag{2.12}$$

as it is visible in figure 2.11.

The data are more scattered than the lift coefficient case and the fitting is difficult, though looking at the results in figure 2.12, it can be seen good approximation at low angles of attack.

Even though a proper fitting of experimental data at low angles of attack up to a height of 2% of chord, a remarkable error is evident when the airfoil incidence reaches 6°. However, as it said before, the angle of attack expected are low, so the model can fit the purpose. The error is probably caused by the scattered nature of the data, both experimental data and the $Z(C_L)$ function.

Two different aspects emerge from the study of the coefficients, the pitching moment increases of a considerable amount. The slope of the lift coefficient curve increases. Moreover, the slope of the pitching moment curve is negative which means that could be present a displacement of the aerodynamic center.

Aerodynamic center displacement The aerodynamic center is the point where C_M is virtually constant, independent of the lift coefficient, i.e. the angle of attack. For low incidences and common airfoils, it is a fixed point between 23% and 25% of the chord behind the leading edge. Using the thin airfoil theory, it is exactly at one quarter chord behind the leading edge for

34
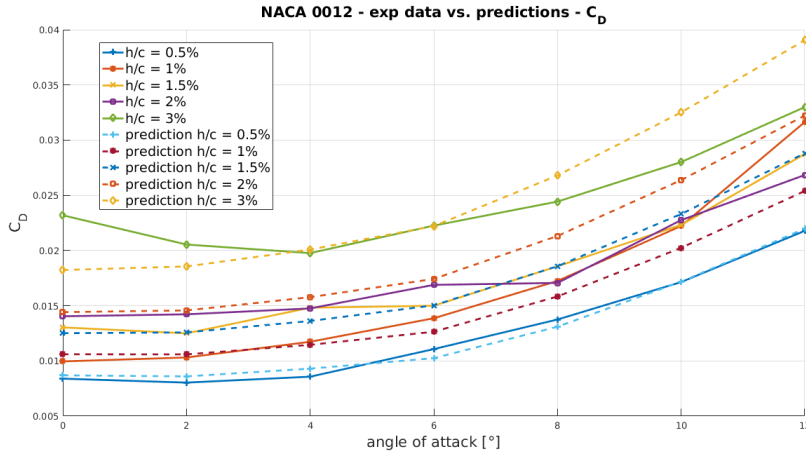
Figura 2.12: Drag coefficient comparison between experimental data and predictions for NACA 0012 with gurney flaps
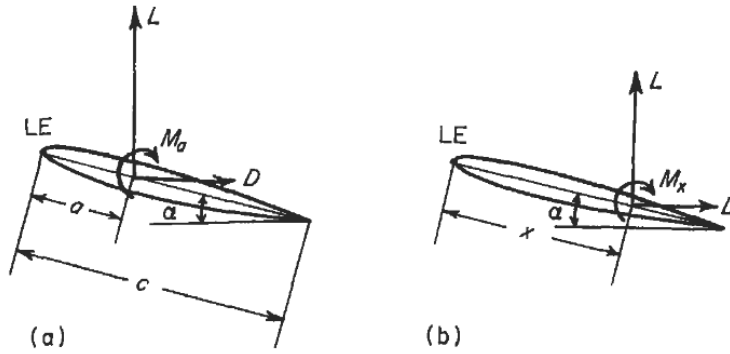
Figura 2.13: Statics of an airfoil

flat and curved plate in inviscid and incompressible flow. The distribution of thickness and the viscosity move it a few percent forward, instead the compressibility tends to move it backwards. In order to evaluate the displacement of the aerodynamic center, it has been used a static theory for the pitching moment that can be found in [11]. The lift, drag and pitching moment about the quarter chord point are known, the moment at desired point can be found using statics, see figure 2.13.

The moments about the leading edge must be the same, and, obviously, the lift and drag are equal in both cases, thus

$$M_{LE} = M_{c/4} - L\,\frac{c}{4}\,cos\alpha - D\,\frac{c}{4}\,sin\alpha = M_x - L\,x\,cos\alpha - D\,x\,sin\alpha. \quad (2.13)$$

The moment about a generic point at distance x from the leading edge is

$$M_x = M_{c/4} - (L\,cos\alpha + D\,sin\alpha)\left(\frac{c}{4} - x\right), \quad (2.14)$$

35

converting to coefficient form by dividing by the dynamic pressure times the reference length[2] squared

$$C_{M_x} = C_{M_{c/4}} - (C_L \, cos\alpha + C_D \, sin\alpha) \left(\frac{1}{4} - \frac{x}{c} \right). \qquad (2.15)$$

To evaluate the position of the aerodynamic center some simplifications can be made, for moderate incidences

$$C_L \gg C_D \quad \text{and} \quad \alpha \ll 1$$

and therefore $C_D sin\alpha$ can be neglected compared with $C_L cos\alpha$. Using the previous approximations

$$C_{M_x} = C_{M_{c/4}} - C_L \left(\frac{1}{4} - \frac{x}{c} \right). \qquad (2.16)$$

Differentiating (2.16) with respect to C_L gives

$$\frac{d}{dC_L}(C_{M_x}) = \frac{d}{dC_L}(C_{M_{c/4}}) - \left(\frac{1}{4} - \frac{x}{c} \right), \qquad (2.17)$$

The position of the aerodynamic center can be found applying his definition to (2.17) and solving for x_{AC}/c, thus

$$\frac{x_{AC}}{c} = \frac{1}{4} - \frac{d}{dC_L}(C_{M_{c/4}}). \qquad (2.18)$$

Therefore, the slope of the moment coefficient with respect to lift coefficient, i.e. angle of attack, must be negative to have an aerodynamic center moved aft of the 25% of chord. This is the case for airfoils equipped with gurney flaps and divergent trailing edges. These former devices are more effective if the airfoil has curvature. In the present work, as forementioned, the airfoil chosen is without curvature, however, the effects are good for moderate angles of attack. In the following section a detailed explanation for the NACA0012 case is done.

Application to NACA0012   Applying equation (2.18) for the chosen airfoil, NACA 0012 equipped with a 2%c gurney flap, it is possible to trace the aerodynamic center position with respect to the change of angle of attack. The results can be seen in figure 2.14. The aerodynamic displacement is not very large in absolute terms, however, the results are good compared to the standard position without gurney flap. The improvements are also located in the region of small angles of attack , indeed, for high angles, the

---

[2]in two dimension there isn't a surface, thus, for example, the lift coefficient is defined $C_L = L/(q\,c)$
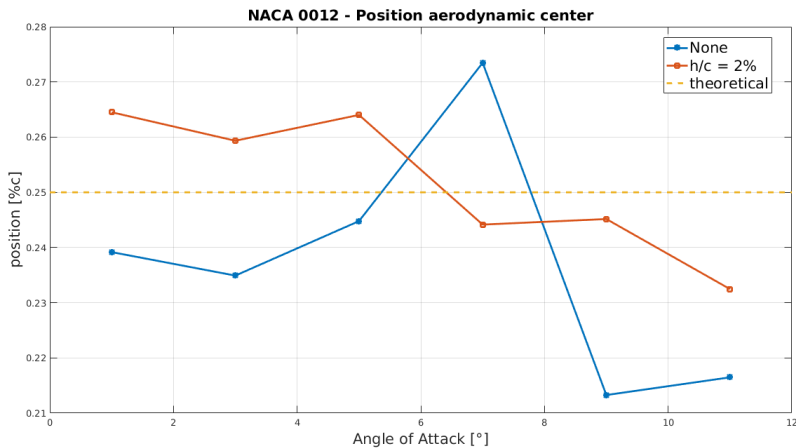
Figura 2.14: Aerodynamic center position for NACA0012 in percentages of chord

panel	angle of attack
panel 1	$-0.55°$
panel 2	$-1.59°$
panel 3	$+0.35°$
panel 4	$+2.79°$
panel 5	$+4.00°$

Tabella 2.1: Baseline blade angles of attack (average on the panel) at $135kts$: panel 1 at root and panel 5 at tip

presence of the gurney is counterproductive from this point of view. Nevertheless, looking at the angles of attack of the model with the standard configuration blade close to the whirl flutter condition, in table 2.1, it is possible to see a low range of operation of the airfoil near the zero angle of attack[3]. Accordingly, the use of the gurney flap is justified.

The aerodynamic center displacement can be improved using cambered airfoils or profiles that show rear loading like RAE or NACA SC. However, the use of the latter requires a new design of the entire propulsive system, a good improvement can be done integrating this modification starting from the initial design. Furthermore, either increases significantly the pitching moment of the entire blade, while the increase of pitching moment using a gurney flap is limited. Moreover, the gurney flap is only a small device attached to the trailing edge, it is possible to think to airfoils that consider the extraction of it only in particular conditions, like at high speeds in a passive way.

---

[3]It is shown the average on the panel.
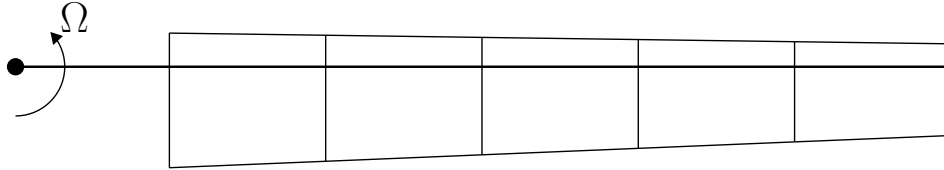
Figura 2.15: Baseline blade representation

2.3 Gurney effects on the tiltrotor model

In this section the effects of the application of the gurney flap on the blade are analysed. It has been chosen to use an airfoil equipped with a 2%c gurney flap. The choice has been done because it is the best compromise in terms of performance and the good approximation of the coefficients using the method described previously. The curve fitting described in the previous section has been used to generate a new airfoil database in a format compatible with MBDyn. The MBDyn database needs the coefficients values from $-180°$ to $180°$ of angle of attack for a range of mach numbers, a method to extend the aerodynamic coefficients with negative angles of attack and mach has been constructed. The method is necessary because the lack of experimental curves in both the conditions. The aerodynamic coefficients curves have been extended to lower and higher angle of attack values using the corrective coefficients functions. The polynomial curves of the corrective coefficients found have been extended following the trends. The application of gurney flap modifies the angle of attack at which the stall arises. Unfortunately there is not a way to predict it, for this reason the angle of attack of the original profile has been kept as the higher values. After the stall, the same coefficients of the original airfoil have been used. The method could introduce some approximation close to the stall angle and for high negative angles of attack. However, the incidence of the blade at high speed is usually low, see table 2.1. The extension to different values of mach number has been done using coefficient of the curve in figure 2.8 and the corresponding C_L in equation 2.4, and then used to construct the other coefficient curves. In this way it has been chosen to not introduce further approximations to generate the curves because the lack of experimental data to validate it. In any case, the maximum mach coefficient of the model is below 0.4, without moving to far outside the zone generally denoted as incompressible.

For the present analysis, the application of the gurney flap has been done using a blade with 5 panels in order to make faster and simplify the parametric study. The baseline line blade geometry has been used. A representation can be see in figure 2.15.

The parametric evaluation has been done in two different ways: gurney flaps applied on a single panel alone and then, on multiple panels at the same time. In both case a simple binary number is used to identify the

presence (1) or not (0) of the gurney from the root (left) to the tip (right).

In order to understand the effects in terms of power required and loads, a parametric analysis has been done at fixed speed, below the baseline whirl flutter speed, and the torque and loads have been studied. Two types of tests have been done, in the first case the thrust has been held at $50\,lbf$ at fixed speed of $135\,kts$. In the second case, the speed has been held fixed always at $135\,kts$, as well as the collective pitch θ_0 for all the modifications. These two different conditions have been chosen to highlight different effects. Keeping fixed the collective angle helps to understand the effects in terms of blade response behavior. While, keeping fixed the amount of thrust allows to understand the variation in the power required and loads.

In table 2.2 and table 2.3 can be found, respectively, the fixed pitch and the fixed thrust summaries. The flap and lag moment in tables are measured at the blade root, the pitch link load is measured inside the rod used to model it. The coning angle has included the precone angle of $2.5°$.

Panels w\gurney	Flap moment $[lbf\,ft]$	Lag moment $[lbf\,ft]$	Pitch link load $[lbf]$	Thrust $[lbf]$	Torque $[lbf\,ft]$	Coning angle $[°]$
0 0 0 0 0	2.58	48.48	8.24	50.12	162.19	2.57
1 0 0 0 0	4.99	40.84	10.67	41.51	138.29	2.17
0 1 0 0 0	4.15	44.24	10.35	44.90	148.59	2.24
0 0 1 0 0	3.97	44.44	10.87	44.74	148.62	2.19
0 0 0 1 0	4.16	42.66	11.32	42.37	142.31	2.23
0 0 0 0 1	3.88	42.60	11.33	41.94	141.93	2.71

Tabella 2.2: Single panel gurney parametric study for fixed pitch

Looking at table 2.2 (fixed pitch analysis) is visible an increase of flap moment with respect to the baseline model in every application of gurney flap. The coning angle is dependent of the position of the gurney. If the device is applied to the tip panel, there is a decrease of the loads on the flexbeam but an increase of the coning angle with respect to the other applications. The reduction of thrust is due to the twist induced by the higher pitching moment. However, the pitch link load increases despite the reduction of thrust.

Panels w\gurney	Flap moment $[lbf\,ft]$	Lag moment $[lbf\,ft]$	Pitch link load $[lbf]$	Thrust $[lbf]$	Torque $[lbf\,ft]$	Coning angle $[°]$
0 0 0 0 0	2.58	48.48	8.24	50.12	162.19	2.57
1 0 0 0 0	3.3	48.30	10.66	49.89	163.13	2.43
0 1 0 0 0	3.12	48.80	10.35	50.00	163.74	2.40
0 0 1 0 0	2.88	49.21	10.85	50.08	164.45	2.36
0 0 0 1 0	2.58	49.57	11.28	50.10	165.24	2.48
0 0 0 0 1	2.09	50.28	11.27	50.53	167.43	2.99

Tabella 2.3: Single panel gurney parametric study for fixed thrust

Looking at the fixed thrust study, the most interesting parameter is the torque. In this case it is visible a general increase of torque for every

application of gurney. The modified panels increase the amount of load on the pitch link as well as on the flexbeam root. A reduction of flap moment is visible for the tip panel however there is an increase of the coning angle.

A summary of the multi-panel application of gurney flaps is visible in table 2.4. There is a general reduction of the lag moment, however, there is an increase of the flap moment on the flexbeam root. Also the pitch link load increases largely, more the the double of the baseline configuration. The coning angle reduces as the increase of the panel equipped with gurney flaps.

Panels w\gurney	Flap moment $[lbf\,ft]$	Lag moment $[lbf\,ft]$	Pitch link load $[lbf]$	Thrust $[lbf]$	Torque $[lbf\,ft]$	Coning angle $[°]$
0 0 0 0 0	2.58	48.48	8.24	50.12	162.19	2.57
0 0 0 0 1	3.88	42.60	11.33	41.94	141.93	2.71
0 0 0 1 1	5.13	38.25	13.93	35.87	127.03	2.41
0 0 1 1 1	6.09	35.84	15.88	32.32	118.94	2.12
0 1 1 1 1	7.06	33.58	17.21	29.24	111.84	1.91
1 1 1 1 1	8.60	28.94	18.73	23.84	97.63	1.66

Tabella 2.4: Multi-panel gurney parametric study for fixed pitch

The fixed thrust analysis is visible in table 2.5. It is interesting to notice the decrease of flap moment. This is due to the reduction of collective angle used to recover the required amount of thrust. There an increase of flap moment but the absolute amount is in general low. The load on the pitch link increases in every situation as well as the torque. The increase of torque is in general limited.

Panels w\gurney	Flap moment $[lbf\,ft]$	Lag moment $[lbf\,ft]$	Pitch link load $[lbf]$	Thrust $[lbf]$	Torque $[lbf\,ft]$	Coning angle $[°]$
0 0 0 0 0	2.58	48.48	8.24	50.12	162.19	2.57
0 0 0 0 1	2.10	50.28	11.27	50.53	167.43	2.99
0 0 0 1 1	1.92	52.21	13.93	51.47	173.32	2.91
0 0 1 1 1	2.04	53.60	16.10	52.18	177.84	2.74
0 1 1 1 1	2.47	54.04	17.71	52.18	179.76	2.60
1 1 1 1 1	3.48	52.08	19.59	49.90	174.63	2.43

Tabella 2.5: Multi-panel gurney parametric study for fixed thrust

As it will be presented in section 3.4, the application of gurney flaps is effective and it will increase the whirl flutter speed. The best solution has the gurney flaps all over the blade span and the whirl flutter speed increases of 14% with respect to the baseline configuration. The increase of maximum speed is, in general, followed by an increase in the loads on the pitch link as shown in the previous parametric analyses. Indeed, for the best configuration in terms of speed, the load is more then double with respect to the baseline blade at fixed speed of $135kts$.

Capitolo 3

Whirl flutter

The chosen aerodynamic modifications to increment the whirl flutter speed in the present work are analysed in this chapter. The blade with swept tips, double sweep angle, anhedral angle at the tip and gurney flaps are studied in the next sections. A parametric study has been done in order to understand the effects of the aerodynamic modifications. The aerodynamic center position, which corresponds to the application point of the aerodynamic forces in MBDyn, has been modified keeping the structure untouched as well as the twist distribution. The mass and the elastic properties of the blade are kept fixed in order to simplify the problem as well as the twist distribution. The effects of swept blade are analysed in more detail to understand the implication in terms of loads and torque.

The blade with a simple swept tip is studied in the first section. Some parametric variations of the model are described and the results are reported. In the second section, the double swept blade is studied. Also in this case, some parametric variation to assess the whirl flutter speed have been done and reported. In the third section the effects of anhedral angles are described. In the fourth section, the increments of whirl flutter speed due to the introduction of gurney flaps are studied. In the last section, a comparison between gurneys and swept blades is done to understand the causes of the whirl flutter speed increments.

3.1 Simple swept blade

In this section a parametric study of the variation of the tip panel aerodynamic center is described. The modifications have been made using the properties of the aerodynamic panels of MBDyn. They give the possibility to change the aerodynamic center position through the use of a generic used-defined function, see [21]. A very generic modification of the aerodynamic center is possible. For the parametric study described here-in, a linear
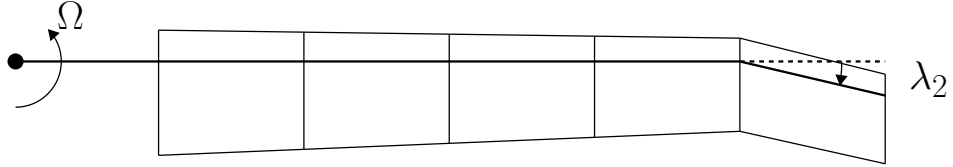
Figura 3.1: Simple swept blade example

function has been used. Only the last panel has been modified introducing the sweep angle, a representation of the modification is shown in figure 3.1.

In the early stages of the work, the rigid version of the rotor has been tested to keep the problem simple. The rigid rotor has a rigid blade with the same geometry of the flexible one as well as a rigid pitch link. However, the infinite torsional stiffness of the rotor cancels the effects of the swept tip described by Acree in [1] and [7]. Then, a flexible pitch link has been introduced keeping the rigid blade. The results were promising but far from the Acree ones. Finally, the flexible blade has been implemented, and the results are visible in the present section. The table 3.1 summarized the results for the different rotors in terms of whirl flutter speed. The different baseline rotors have slightly different whirl flutter speed, for this reason in table is present the speed increment in percentage with respect to the corresponding rotor with baseline blades.

Rotor type	λ_2	Whirl flutter speed	% with respect to corresponding baseline	$\Delta\theta_0$
	[°]	[kts]		[°]
Full rigid	25	146	2.8	0.0
Rigid blade, flex pitch link	25	170	13.4	+1.3
Full flexible	25	180	20.8	+1.9

Tabella 3.1: Whirl flutter speed comparison for different rotor models

The results indicate that the increase of whirl flutter speed due to the use of swept blades is related to the torsional deformation of the rotor system. The introduction of a torsion at the blade tip modifies the elastic twist of the blade. This reduces the asymmetric force that is responsible for the whirl flutter, as described in the introduction chapter.

As explained before, the baseline model has proven to become unstable faster with a fixed thrust trim condition, for this reason the effects of the swept tips on the whirl flutter speed has been studied at fixed thrust. For every sweep angle a variation of the collective pitch has been mandatory to restore the right amount of thrust.

As it has been done previously for the introduction of gurney flaps, two different trim conditions at fixed speed of 135 kts have been used: one with

42

fixed thrust and one with fixed pitch. The summary of the former is visible in table 3.2.

λ_2 [°]	Flap moment [$lbf\,ft$]	Lag moment [$lbf\,ft$]	Pitch link load [lbf]	Thrust [lbf]	Torque [$lbf\,ft$]	Coning angle [°]
0	2.58	48.48	8.24	50.12	162.19	2.57
5	2.85	48.29	9.55	49.98	161.97	2.47
10	3.05	48.27	10.70	50.01	161.93	2.41
15	3.27	48.03	11.74	49.84	161.40	2.31
20	3.35	48.43	12.72	50.35	162.92	2.25
25	3.35	49.5	13.65	51.00	165.60	2.26

Tabella 3.2: Swept tip blade parametric study summary at fixed thrust

The only parameter that really changes is the load on the pitch link. Fixing the thrust, the torque has not changed, indeed, the airfoils are still NACA0012. The coning angle is slightly reduced even if the flap moment is slightly increased.

Instead, the results for fixed pitch condition are summarised in table 3.3.

λ_2 [°]	Flap moment [$lbf\,ft$]	Lag moment [$lbf\,ft$]	Pitch link load [lbf]	Thrust [lbf]	Torque [$lbf\,ft$]	Coning angle [°]
0	2.58	48.48	8.24	50.12	162.19	2.57
5	5.41	37.27	9.53	37.35	124.33	2.07
10	7.36	29.05	10.42	28.50	98.15	1.73
15	8.82	23.12	11.09	21.87	78.58	1.48
20	9.96	18.45	11.74	16.64	63.14	1.25
25	10.90	14.60	12.06	12.32	50.45	1.10

Tabella 3.3: Swept tip blade parametric study summary at fixed pitch

Keeping fixed the collective angle allows to watch the effects on the blade with swept tip. The thrust is drastically reduced by the introduction of the swept tip. As explained by Acree in [7], the swept tip generates a pitch down moment that twist down all the blade. The consequence is that the thrust is reduced but the loads on the pitch link increases. Due to the twist of the blade (geometric and induced by the swept tip) reduces the coning angle. For this reason the flap moment calculated at the flexbeam root increases. It also depends on the lift distribution.

A parametric study on the whirl flutter velocity has been also done. Following the results of the baseline model, the chosen trim condition is at fixed thrust. The introduction of the swept tips generates a decrease of thrust, so a modification of the collective pitch has been used to recover the required propulsive force. As for the baseline model, the same perturbation force has been used, see 1.2, as well as the movement checked. In table 3.4 are reported the numerical results, in figure 3.2 are reported the percentage increments with respect to the baseline configuration.

λ_2	Whirl flutter speed	$\Delta\theta_0$
$0°$	$149\,kts$	$+0.00°$
$5°$	$155\,kts$	$+0.45°$
$10°$	$165\,kts$	$+0.85°$
$15°$	$169\,kts$	$+1.25°$
$20°$	$178\,kts$	$+1.60°$
$25°$	$180\,kts$	$+1.90°$

Tabella 3.4: Summary of the parametric study of swept tip blade

λ_1	λ_2	Whirl flutter speed	$\Delta\theta_0$
$0°$	$0°$	$149\,kts$	$+0.00°$
$2°$	$10°$	$97\,kts$	$-1.20°$
$3°$	$25°$	$95\,kts$	$-1.80°$
$5°$	$25°$	$68\,kts$	$-2.60°$

Tabella 3.5: Summary of the parametric study for a double swept blade

The results are in good agreement with the work of Acree, [1]. The introduction of a swept blade has been capable of increasing the speed at which the whirl flutter occurs up to 20.8%.

3.2   Double swept blade

The effects of a double swept blade are reported in this section. Previous studies [7] show that a single forward sweep angle is penalizing. The aeroelastic response of a tiltrotor with a double swept blade has never been studied, for this reason a parametric study has been done and described here-in. A schematic drawing of the blade geometry and parameters definition is shown in figure 3.3.

Since the initial results were not promising, the λ_2 angle has been set to higher values. The parameters used and the respectively results are shown in table 3.5.

The results are not promising. The displacement of the aerodynamic center of the first part of the blade has a negative effect on the stability of the system. The effects of the forward swept are higher than the effect of the backward swept tip. It is important to highlight that only the last panel is swept backward and four panels have their aerodynamics center in front of the pitch axis. Looking at the collective pitch angle modifications is clear that the thrust increases as the increase of forward sweep angle. For this reason the correction is negative. This attitude could be expected looking at the solutions found for the simple tip swept blade, where the variation of thrust is negative. The analysis of the loads has not been done because the negative results on the whirl flutter speed.
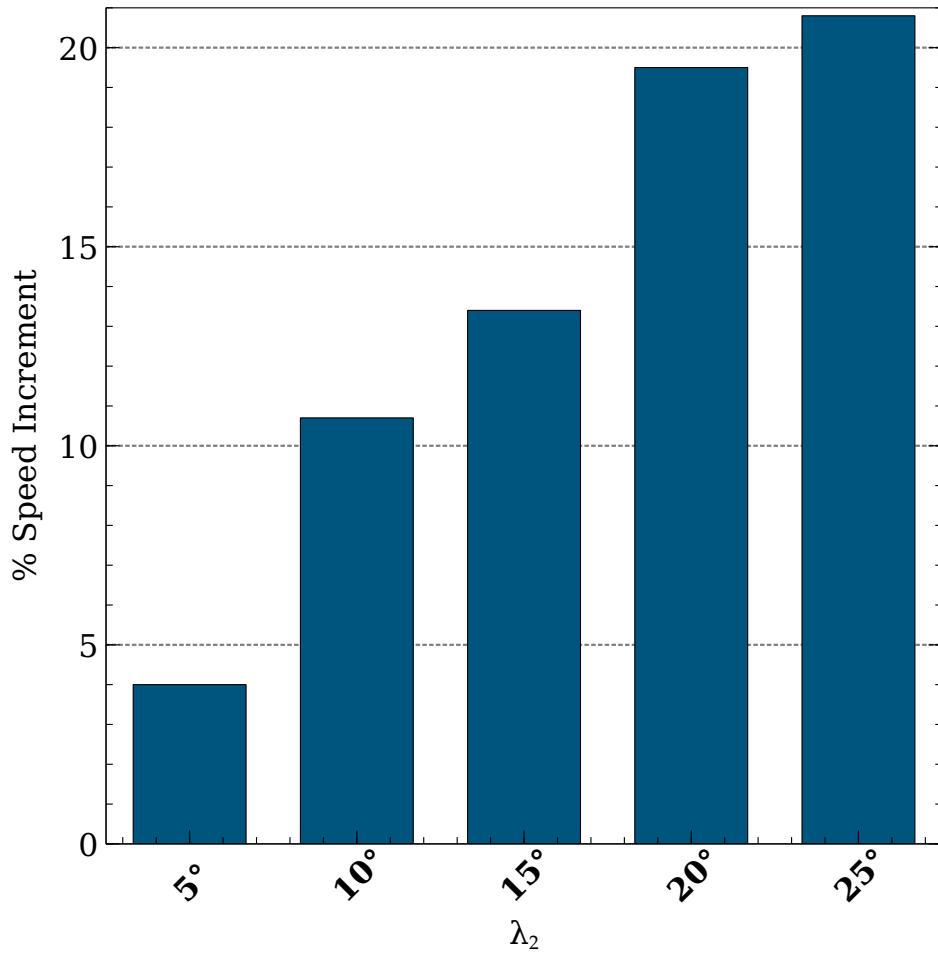
Figura 3.2: Speed increments for rotor with swept tip blades
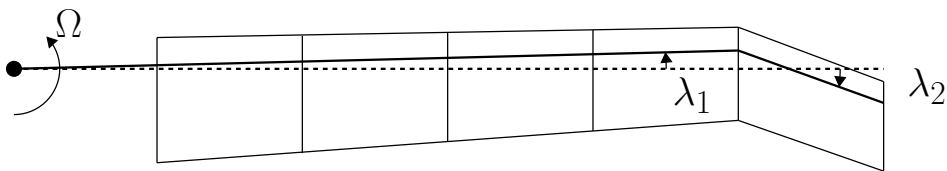
Figura 3.3: Representation of blade and the parameters used
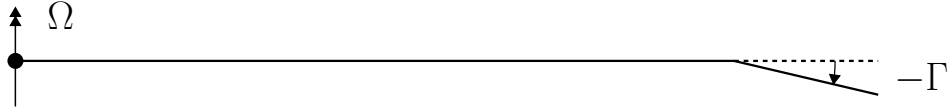
Figura 3.4: Anhedral angle definition

3.3   Blade with anhedral angle on the tip

In this section the effects of blades with anhedral angle at the tip are described. Following the same fashion used for the simple swept blade, only the last panel has been modified. The definition of the anhedral angle and a representation of the blade can be found in figure 3.4.

As previously, the study has been done fixing the amount of thrust. To recover it a variation of collective pitch has been used. Also in this case, the movements checked have been the wing tip movements and the blade movements in the hub reference frame. The force to perturb the system has been the same of the simple swept case.

Few angles have been tested, the whirl flutter velocity tends to decrease. The results are summarized in table 3.6.

Γ	Whirl flutter speed	$\Delta\theta_0$
$0°$	$149\,kts$	$+0.0°$
$-2.5°$	$149\,kts$	$+0.0°$
$-5.0°$	$147\,kts$	$+0.0°$
$-10.0°$	$142\,kts$	$+0.0°$

Tabella 3.6: Summary for blades with anhedral

Several interesting results can be seen. First, the application of anhedral does not need a variation of a collective pitch angle, at least using this simple aerodynamic model. There is a reduction of whirl flutter speed as the increase of anhedral angle. This behaviour is opposite to the one of [31], however, the introduction of anhedral in those studies has been done modifying the structure as well. As stated by Acree in [7], the increase of system stability is given by the offset produced by the mass droop. So, neglecting the effect of the structure is counterproductive like shown. For this reason the introduction of the anhedral angle has been skipped for the optimisation process. Since there is not an increase of the whirl flutter speed, a study on the variation of torque and loads has not been done.

3.4   Gurney flaps

The effect of gurney flaps are reported and analysed in this section. The same fashion of the previous analysis has been used: a fixed thrust trim

condition has been utilised and the collective pitch has been changed to recover the right amount of thrust. Also the perturbation force has been kept equal to the baseline study. The parametric evaluation has been done in two different ways: gurney flaps applied on a single panel alone and then, on multiple panels at the same time. In both case a simple binary number is used to identify the presence (1) or not (0) of the gurney from the root (left) to the tip (right). For single panel case, the results are reported in table 3.7.

Panel w\gurney	Whirl flutter speed	$\Delta\theta_0$
00000	149 kts	+0.00°
10000	153 kts	+0.50°
01000	153 kts	+0.37°
00100	153 kts	+0.31°
00010	151 kts	+0.41°
00001	149 kts	+0.30°

Tabella 3.7: Summary of the parametric study of gurneys on a single panel

The introduction of gurney flaps on some panels is capable of increasing the whirl flutter speed of the model. The two extreme cases have contrasting effects. The application of the gurney flap at the blade tip panel does not increase the stability of the system. Instead, using a airfoil with gurney flap at the root increases of a small amount the speed. The reason stands in the twist induced by the airfoils with gurneys[1]. The twist induced by the tip does not propagate all over the blade, vice versa if the twist is induced at the blade root. Thanks to that, the twist generated by the root panel is capable of increasing the stability.

The summary of the multi-panel study is visible in table 3.8.

Panel w\gurney	Whirl flutter speed	$\Delta\theta_0$
00000	149 kts	+0.00°
00001	149 kts	+0.30°
00011	151 kts	+0.80°
00111	155 kts	+1.18°
01111	161 kts	+1.70°
11111	170 kts	+2.70°

Tabella 3.8: Summary of the parametric study of gurneys on multi-panels

There is an increase of whirl flutter speed for every modification. In general the speed gain is low, however it has been proven that the use of gurneys can improve it. Another important aspect is that, nevertheless the

---

[1]A detailed explanation of the phenomenon behind the increase of stability is provided in the following section.

increase of lift coefficients due to the gurneys, the collective pitch has to be increased to recover the right amount of thrust. This is due to the increase of pitching moment that tends to twist pitch-down the blade. More twist is induced to the blade, more the stability region of the system increases.

3.5 Swept blades and gurney flaps comparison

The simple swept blade and the gurney flaps, both capable of increasing the whirl flutter speed, are compared in this section. The purpose is to understand the phenomena behind the increase of system stability augmentation. The two solution are compare to the baseline model. Only the extreme solutions have been compared: swept tip of $25°$ and the blade with gurney flaps on every panel. The velocity has been fixed at $135\,kts$ and the blade coefficient distributions are compared in two conditions like the previous analyses, at fixed thrust and at fixed pitch. The fixed pitch condition helps to understand what happens when one of the solution is used. The fixed thrust analysis shows the effect of the implementation. However, in this case there is not a perturbation force because the aeroelastic stability was already studied. The causes of the increase of stability are studied here.

In the following figures are reported the forces generated by the aerodynamic panels with respect to the elastic axis of the blade against the radius station from root to tip.

The various distributions for fixed pitch angle are reported in figure 3.5. First of all, it is important to notice the peculiar behaviour of the lift distribution of every model. The lift starts at the root of the blade with a negative value then decreases up to a minimum around $1.6\,ft(42\%R)$ and then starts to increase. This particular distribution is the results of a compromise between performances during hover and cruise flight. Indeed, as reported by Droandi in [8],

> " [...]In fact, the need to have also this part collaborating (and therefore not stalled) in the helicopter mode (where much more traction is required) leads to a blade twist quite lower respect to the need of a propeller, so producing negative incidences in aeroplane mode.[...]".

The thrust is reduced for both the cases with modifications and the blades with gurneys have higher lift almost in every portion with respect to the swept blade. Looking at the angles of attack, however, the blade with gurneys has lower angles, this means that the lift is recovered by the increase of sectional lift coefficient due to the gurney. From the angle of attack curves is also evident that the pitching moment introduced by the gurney flaps is capable of elastically twisting more then the swept tip at least in this case. It is possible to understand the elastic twist of the blade analysing the trend

variation on the angle of attack. The modified blades have higher elastic twist at the blade tip. The results is a reduction of the lift generated in this region. The angles of attack of the swept blade experiences a plateau at the same radius station of the increasing of pitching moment. It is evident that the pitch moment in the gurney case is distributed, instead, for the swept blade is concentrated only in small portion (where there is the sweep).

The summary of the study conducted at fixed thrust is visible in figure 3.6. Also in this case, the lift distributions of the modified blades have reduced production of thrust near the blade tip. In order to compensate this reduction of lift, the pitch angles have to be increased, consequently the angles of attack increase with respect to the previous analysis at fixed pitch. The modified blades produce more lift near the root with respect to the baseline model. The swept blade shows an interesting behaviour: the angles of attack near the tip starts to reduce from the point where the sweep is introduced. The higher collective pitch needed to recover the thrust introduced more pitch down moment that increase the elastic twist of the blade up to reducing the angle of attack. To recover the thrust loss at the wing tip, the lift distribution of the swept blade is higher of the gurney one in the central region.

The study reported in this section confirms that a pitch down moment that creates an elastic twist of the blade has a stabilising effect. It is evident that the elastic twist of the blade is the responsible of the stability augmentation of the system. However, the aerodynamic modifications able to twist the blade are always followed by higher loads on the control chain and at the blade root.
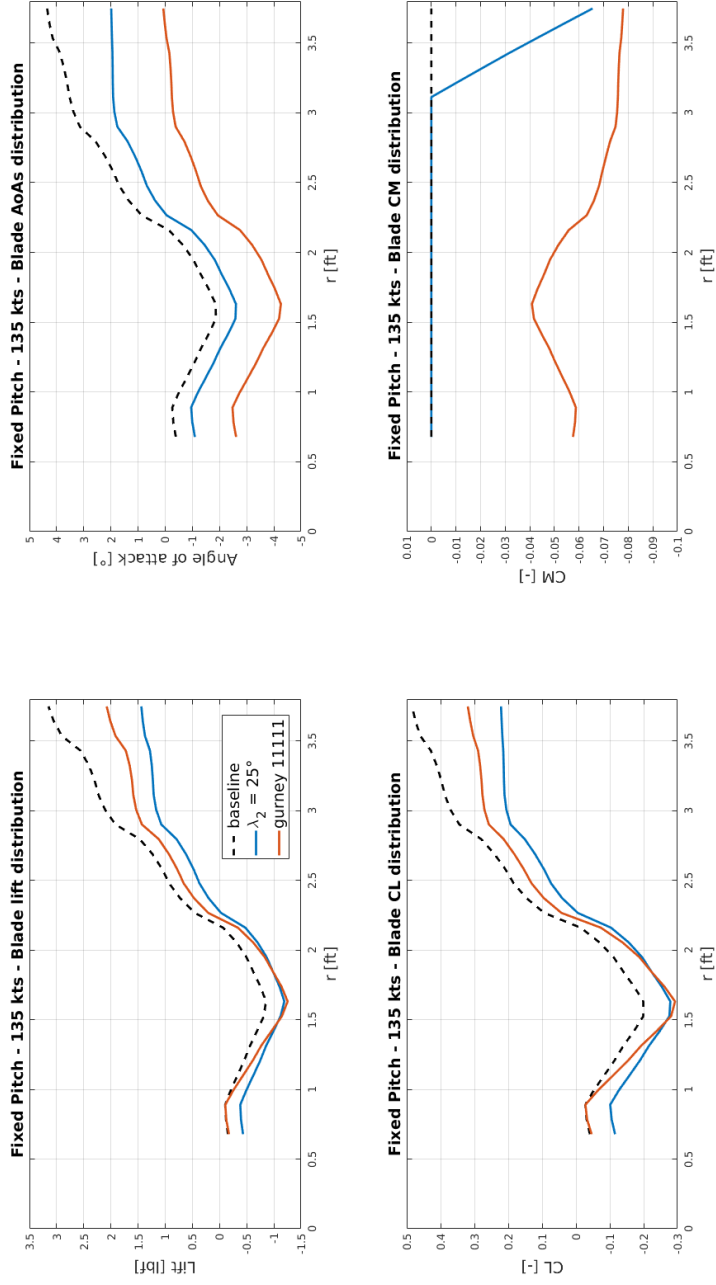
Figura 3.5: Aerodynamic distribution on the blade for fixed collective pitch angle
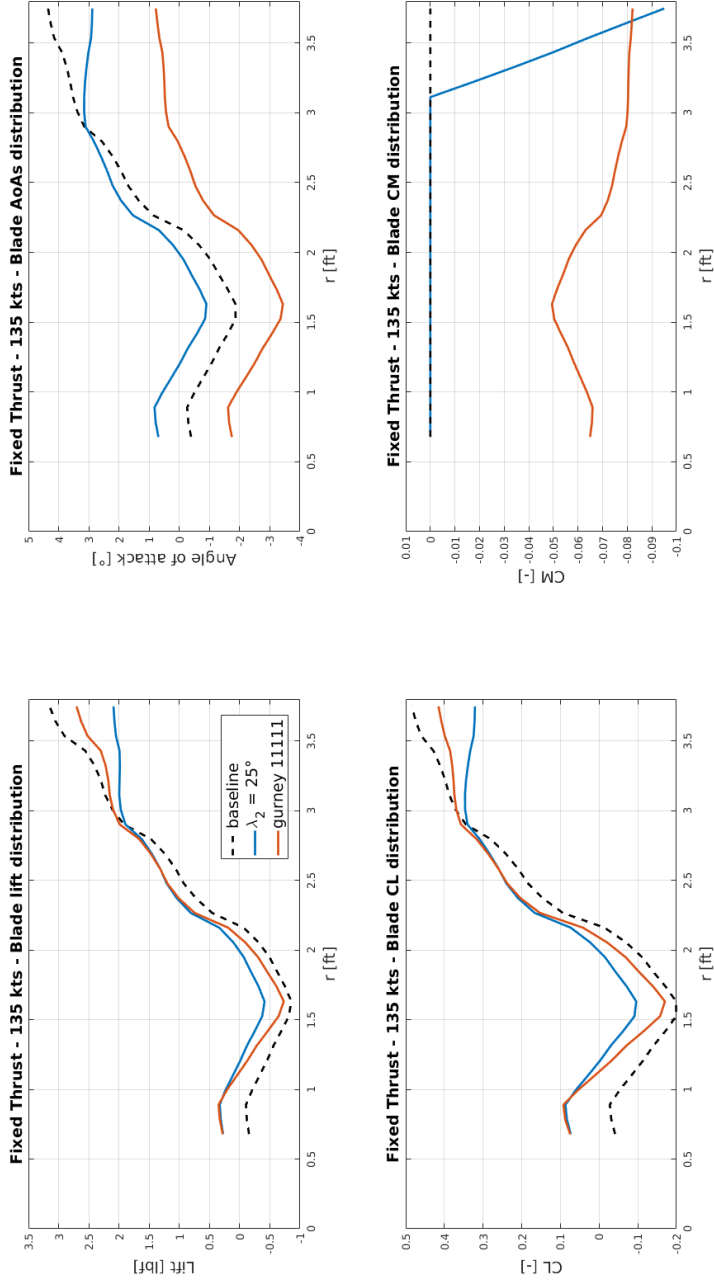
Figura 3.6: Aerodynamic distribution on the blade for fixed thrust

Capitolo 4

Optimisation

The chapter describes the optimisation procedure used in order to find the best solution in terms of whirl flutter velocity combining the results of the previous chapters. The optimisation values are here-in described and discussed as well as the algorithm. A method to recover the correct amount of propulsive force has been developed and it is discussed here due to the use of fixed thrust trim condition.

In the first section of the chapter, the genetic algorithm is briefly explained highlighting the pros and cons, and the reason behind its choice in the present work. The problem formulation is described in the second section as well as the objective function definition and the parameters bounds. In the last section the results of the optimisation process are reported and the comparison with the other models previously analysed is discussed.

4.1   Genetic algorithm

The choice of the optimisation algorithm depends on the problem analised. Several parameters contribute to the decision of the right method to be used: the number of variables, the shape of the objective function, the possibility to have analytical derivatives, etc..

A good starting point is the shape of the objective function, indeed, if a single minimum is expected, it is possible to use gradient based methods. The gradient requires the computation of the derivatives, they can be done analytically or numerically. In the present work, the use of gradient based method is not possible due to the difficulties to compute the derivatives. Also a non monotonic behavior of the objective function is expected (see figure 4.1 for an example of non monotonic search space), for these reasons a genetic algorithm has been used.

The genetic algorithm (GA) is stochastic meta-heuristic optimisation method in theory capable of optimise an objective function also in presence of local minima (example of search space with local minima in figure 4.1).

Figura 4.1: Example of non monotonic search space (from [30])
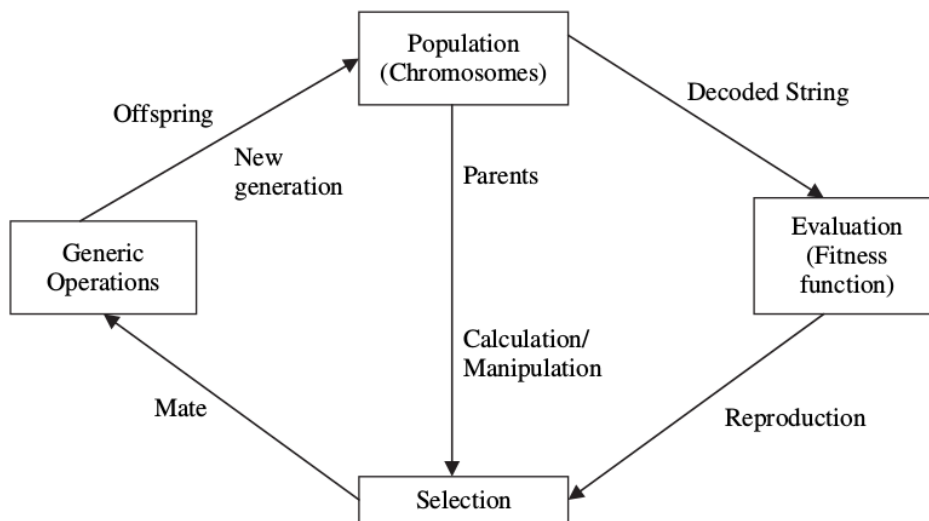
Figura 4.2: Genetic algorithm cycle (from [30])

It has been invented by John Holland in the 1975 in his book "Adaption in natural and artificial systems". Like most of the stochastic methods, GAs do not ensure to find the global optimum solution to a problem, they are satisfied with finding "acceptably good" solutions. They are inspired by the natural selection that belongs to the large class of evolutionary algorithms.

GA handles a population of possible solutions. Each solution is represented through an individual. A set of reproduction operators has determined. Reproduction operators are applied directly on the individuals, and are used to perform mutations and recombinations over solutions of the problem. Selection is supposed to be able to compare each individual in the population. Selection is done using a fitness function. Each individual has an associated value corresponding to its fitness function evaluation. The optimal solution is the one which maximises the fitness function.

Once the reproduction and the fitness function have been properly defined, a GA is evolved according to the same basic structure. It starts by generating an initial population of individuals. This first population must offer a wide diversity of genetic materials. The search pool should be as large as possible to that any solution of the search space can be engendered. Generally, the initial population is generated randomly. Occasionally the solutions may be "seeded" in areas where the optimal solutions are likely to be found. The genetic algorithm loops over an iterative process to make the population evolves. A representation of the GA cycle is shown in figure 4.2.

Each iteration consists of the following steps:

- **Selection**: a portion of the individuals is selected for reproduction. The selection is done using a fitness-based process, where fitter solu-

tions (as measure by the fitness function) are typically more likely to be selected.

- **Reproduction**: offspring are bred by the selected individuals generating a second or successive generation population. A combination of genetic operators, crossover and mutation operators, are used. In order to have a faster calculation elistism is used: the best organisms from the current generation are kept unaltered to next generation, improving the convergence of the solution.

- **Evaluation**: the fitness of the new individuals is evaluated.

- **Replacement**: in the last step, individuals from the old population are killed and replaced by new ones.

The algorithm is stopped when the population converges toward the optimal solution.

4.2 Problem formulation and objective function

The mathematical formulation of the generalised constrained optimisation problem can be written as follow:

Minimise:

$$\boldsymbol{F}(\boldsymbol{x}) = (f_m(\boldsymbol{x}))^T, \qquad m = 1, ..., M, \qquad (4.1)$$

subject to:

$$
\begin{aligned}
x_i^{LB} \leq x_i \leq x_i^{UB}, & \qquad i = 1, ..., N, \\
g_j(\boldsymbol{x}) \leq 0.0, & \qquad j = 1, ..., J, \\
h_k(\boldsymbol{x}) = 0.0, & \qquad k = 1, ..., K
\end{aligned}
$$

where $\boldsymbol{x} = (x_1, ..., x_N)^T$ is the design variable array (or individual) and $\boldsymbol{F}(\boldsymbol{x})$ is the objective function that is composed by M scalar quantities, where M is the number of selected objectives. In case of scalar objective function, which is the case of the here-in optimisation, $M = 1$. The design variable space is defined imposing the upper and the lower bounds through $\boldsymbol{x}^{UB}$ and $\boldsymbol{x}^{LB}$. The solution is a feasible solution inside the feasible solution space if it respects the linear inequality $g_j(\boldsymbol{x})$ and equality $h_k(\boldsymbol{x})$ constraints.

In the present work, the blade design variables array $\boldsymbol{x}$ is defined as follow:

$$\boldsymbol{x} = (x_{peak}, y_{peak}, \lambda_2, GI_1, ..., GI_{10})^T, \qquad (4.2)$$
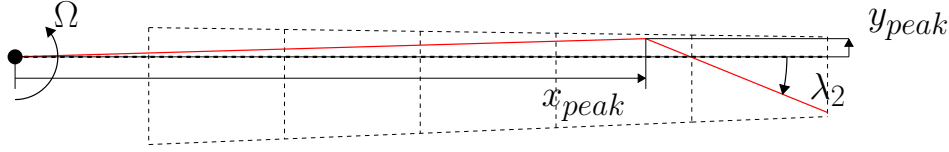
Figura 4.3: Blade variables definition: the aerodynamic center locus is in red.
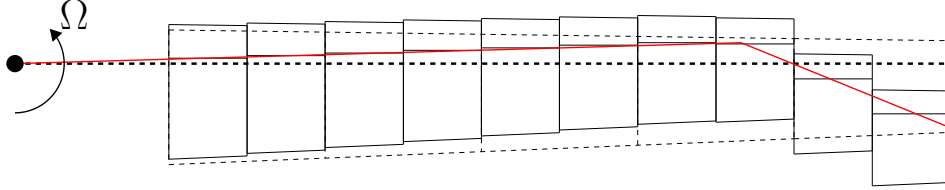
Figura 4.4: Blade variables definition: implementation in MBDyn

and includes the position of the blade aerodynamic center locus peak,

$$(x_{peak}, y_{peak}),$$

the tip sweep angle,

$$\lambda_2,$$

and the Gurney Indeces

$$GI_i, \qquad\qquad i = 1, .., 10,$$

that defines the presence of the gurney or not. A visualization of the aerodynamic center locus can be found in figure 4.3 and the MBDyn implementation is visible in figure 4.4.

In particular, 10 airfoil sections have been identified along the blade span in order to able to have more flexibility in the geometry modifications [1]. The total number of variables is 13. The original blade twist distribution has been kept in order to reduce the complexity of the problem. In order to simplify the handling of the thrust variation, the airfoil sections are moved entirely, as shown in figure 4.3. It has been tested that the effects of using a linear function to modify the aerodynamic center position of the panel can be approximated moving the entire panel taking the position of the aerodynamic center interpolating the linear function. The details of the validation can be found in appendix C.

The upper and lower bounds for the variables can be found in table 4.1. The limits of the peak are given in order to enforce a double swept geometry on the blade as well as the λ_2 bounds. The latter is also kept lower in order to enforce the convergence of the solution as well as the feasibility. Increasing

---

[1]Using more airfoil sections does not change the response and the behaviour of the system.

Lower bound	Variable	Upper bound
$0.6\,R$	x_{peak}	$0.9\,R$
$0.0\,R$	y_{peak}	$0.05\,R$
$0.0°$	λ_2	$26.5°$

Tabella 4.1: GA variable bounds

further the upper limits, could change drastically the mass and stiffness properties of the blade, that here-in are kept constant for simplicity.

The objective of the optimisation process is to increase the whirl flutter speed using an advanced geometry blade and gurney flaps. In order to find the best configuration, the optimisation process has to deal with different limitations of the complex system studied and the multibody software used. The trim condition is a general problem in every situation involving a rotor. For this reason, nevertheless the objectives is to increase the whirl flutter speed, a fixed speed and fixed thrust trim condition is used, allowing to keep simple calculation both in trim and aeroelastic response. The objective function has been defined looking at the most common displacements excited by the whirl flutter. These displacements have been studied on the baseline configuration as explained in 1.2.1. All movements of the wing, out-of-plan bending, in-plane bending and torsion, have been tracked as well as the flapping of the blades. The tiltrotor model is trimmed at fixed speed of $135\,kts$ and the exciting force, summarised in table 1.5, is applied at the wing tip. The speed of $135\,kts$ has been chosen to have fair comparison for every blade geometry, indeed, the baseline model is also stable at this velocity. The exponential decays of the movements are fitted using an exponential function as already explained. Indeed, the exponent can be related to the damping of the system. In this way it is simple to define an objective function:

$$f(\boldsymbol{x}) = \sum_{n}^{4} w_i \xi_i \qquad (4.3)$$

where w_i are the weights ($w_i = 0.25$) and ξ_i the exponent of the movements chosen.

The method used fits perfectly in the context of genetic algorithm optimisation because it is fast and simple to implement. Indeed, the combination of multibody software and genetic algorithm requires a large amount of time for the computation, for this reason, every simplification of the process is a clear advantage.
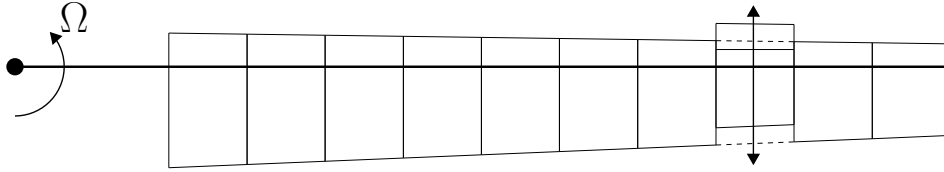
Figura 4.5: Representation of the panel movements used to study the effects on the thrust

4.2.1 Thrust variation analysis

The optimisation is set up using a semi-model of a tiltrotor trimmed at fixed speed and it has to have fixed thrust. Using the baseline model, a thrust of $50\,lbf$ has been chosen. However, the introduction of sweep and airfoils equipped with gurney flaps changes the amount of thrust produced by the rotor at fixed collective pitch, as visible in the previous chapters. In order to recover the right amount of thrust a simple and effective approach has been constructed.

Due to the strip theory used by MBDyn, the effects of changing the position of a single section do not influence aerodynamically the other panels. For this reason a simple superposition effect of the thrust variation has been used.

The superposition principle is valid for the aerodynamic model, however, the modification of the aerodynamic panels changes the response of the system itself but the variation of movement and angle of attack has low impact.

The introduction of this modification of the blade geometry has been studied at the velocity for the optimisation analysis, $135\,kts$. The study has been done varying the position of every panel with respect to the pitch axis. Every section has been moved forward and backward two times to construct a curve of the changing thrust. A simple representation of the panel movements can be seen in figure 4.5. The curves have been fitted using a polynomial, in this way, entering with the displacement of the single panel, it is possible to predict the variation of thrust generated. Then, acting on the collective pitch is possible to recover the right amount of thrust. Unfortunately, the use of gurney flaps changes the aforementioned curves, so the same analysis previously described has also been done with the introduction of gurney.

For clarity are reported here the curves of the tip panel for both the conditions to show an example, with gurney flap and without it:

$$\Delta T_{clean} = 5030.31 y_{10}^3 + 1264.29 y_{10}^2 + 267.78 y_{10} \qquad (4.4)$$

$$\Delta T_{w/gurneys} = 8899.77 y_{10}^3 + 1941.74 y_{10}^2 + 407.92 y_{10} - 1.74 \qquad (4.5)$$

where the y_{10} is the displacement of the tip panel with respect to the pitch axis, and ΔT the variation of thrust. A graphical representation is

provided in figure 4.6. It is clear that the curve due to the simple displacement of the panel cross the zero. Instead, the curve for the use of panel with gurney flap has an offset. The presence of the gurney decreases the thrust produced by the blade introducing a twist due to the aerodynamic pitching moment. It is also visible that, for this panel, moving the panel forward has more effects on the thrust than moving backward of the same quantity.
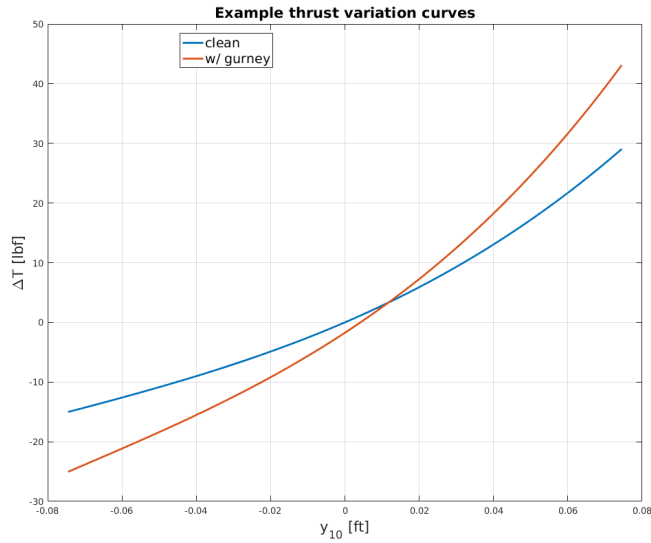
Figura 4.6: Example of thrust variation curves

The curves of every panel are used together to predict the collective pitch to recover the right amount of thrust.

4.3   Results

The genetic algorithm has been run on a Intel Core 2 E7500 and lasted between 48 to 72 hours[2]. The convergence has been reached after 30 generations and 600 simulations. The optimum result found can be seen in figure4.7, where the panels equipped with gurney flaps are represented in red.

The optimal shape scored -2.790 in the fitness function. The most swept blade tested , with $\lambda_2 = 25°$, scored -2.377 and the baseline model scored -0.9645. As expected, the application of gurney flaps and advanced geometry blades increases the damping of the system. The blade has a forward sweep angle of $0.83°$ and the backward sweep angle of $25.71°$. The peak coordinates are $(62.2\%R, 0.9\%R)$. As shown by the parametric study

---

[2]Several analyses have been performed but only one is reported here. The objective function has several local minima one close to the other in terms of objective value.
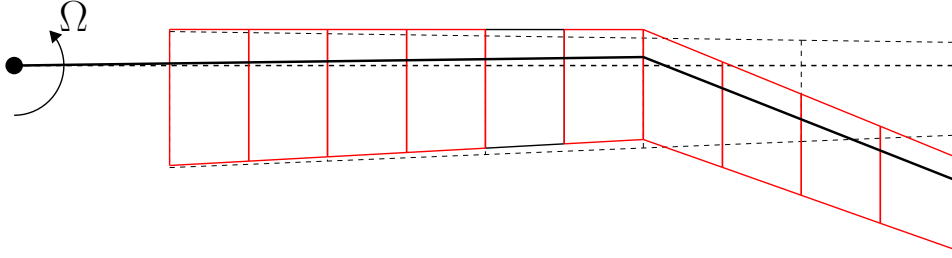
Figura 4.7: Optimal aerodynamic blade (in red the panels equipped with gurney flaps)

model	Whirl flutter speed	Speed increment	$\Delta\theta_0$
Baseline	$149 kts$		$+0.00°$
Gurney 11111	$170 kts$	$+14.1\%$	$+2.70°$
$\lambda_2 = 25°$	$180 kts$	$+20.8\%$	$+1.90°$
Optimal blade	$198 kts$	$+32.9\%$	$+6.30°$

Tabella 4.2: Whirl flutter speed comparison for optimal blade

on the double swept blade, the use of relatively high forward sweep angles is destabilising. The optimisation confirms this result and only a very small forward sweep is present on the optimal blade. The region of the blade moved backward with respect to the feathering axis is large and corresponds to almost the last 40% of the blade surface. The λ_2 angle corresponding to this particular configuration is $25.71°$. There is not a particular scheme for the gurney disposition. The non linearity of the system generates a "flat" objective function space with several minima with close objective value but different gurney dispositions. Introducing the gurney flaps increases the damping of the system, however, the major contribution is given by the swept section as evince by previous analyses. Several optimisations have been performed and the same behaviour has been found. The blade geometry is almost the same but the position of the gurneys can slightly change.

The whirl flutter test on the optimal blade has conducted to a velocity of $198 kts$. The whirl flutter speed comparison with the cases studied in detail in section 3.5 is visible in table 4.2. The blade designed using the genetic algorithm is capable of increasing the speed up to $198 kts$, that means an increment of 33% with respect to the baseline model.

In order to understand the loads and power implications of the optimal blade, a study at fixed pitch and fixed thrust have been done and the results have been compared to the other cases. Like the previous studies, two conditions have been identified: one at fixed pitch angle and one at constant thrust.

The loads at constant collective pitch are reported in table 4.3.

The swept region on the blade induces so high twist up to generates

Model	Flap moment [lbf ft]	Lag moment [lbf ft]	Pitch link load [lbf]	Thrust [lbf]	Torque [lbf ft]	Coning angle [°]
Baseline	2.58	48.48	8.24	50.12	162.19	2.57
Gurney 11111	8.60	28.94	18.73	23.84	97.63	1.66
$\lambda_2 = 25°$	10.90	14.60	12.06	12.32	50.45	1.10
Optimal blade	16.92	−6.78	22.54	−16.08	−20.57	0.62

Tabella 4.3: Optimal blade study summary at fixed pitch

negative thrust. The results is emphasised by the high speed encountered by the rotor. Indeed, like for the other cases, a small change in the collective pitch, and so on the angles of attack, alters the thrust of a large quantity. Also the region of negative lift on the blades, see 3.5 and 3.6, is responsible for that. Indeed a small change in the collective pitch can change the sign of the lift coefficient creating a large change in the thrust.

Instead, the results at constant thrust are visible in table 4.4. As the other cases there is an increase of loads in all the principal components of the rotor. The flap moment is almost two times the baseline one. The lag moment is increased with respect to the baseline and the other models as well, but the difference is limited. The load on the pitch link is four times the baseline load. This could be a problem for the control chain. Also the torque required is higher. The torque values are high, however, in order to restore the thrust a collective pitch variation of 6.3° has been used, increasing the drag coefficient of the sections. Also the introduction of the gurney flaps has an impact on the torque value. Some limitation in terms of power required could arise. However, optimal blade is capable of increasing the whirl flutter speed to higher limits.

Model	Flap moment [lbf ft]	Lag moment [lbf ft]	Pitch link load [lbf]	Thrust [lbf]	Torque [lbf ft]	Coning angle [°]
Baseline	2.58	48.48	8.24	50.12	162.19	2.57
Gurney 11111	3.48	52.08	19.59	49.90	174.63	2.43
$\lambda_2 = 25°$	3.35	49.5	23.65	51.00	165.60	2.26
Optimal blade	4.90	51.74	31.58	50.55	175.59	1.84

Tabella 4.4: Optimal blade study summary at fixed thrust

In order to comprehend in detail the differences with respect to the baseline model, a study of the forces acting on the blade has been done. The aerodynamic force has been decomposed in the two components, one perpendicular and one in the plane of the rotor disc. The sum of the force perpendicular to the rotor disc is the thrust produced. Instead, the in-plane force is a composition of the lift and the drag produced by the blade, in particular situations, the lift is the major contributor. Also in this case, the analyses have been performed as usual at fixed thrust, fixed pitch and whirl flutter conditions[3].

---

[3]Due to the use of 10 airfoils section, the application points of the force are slightly
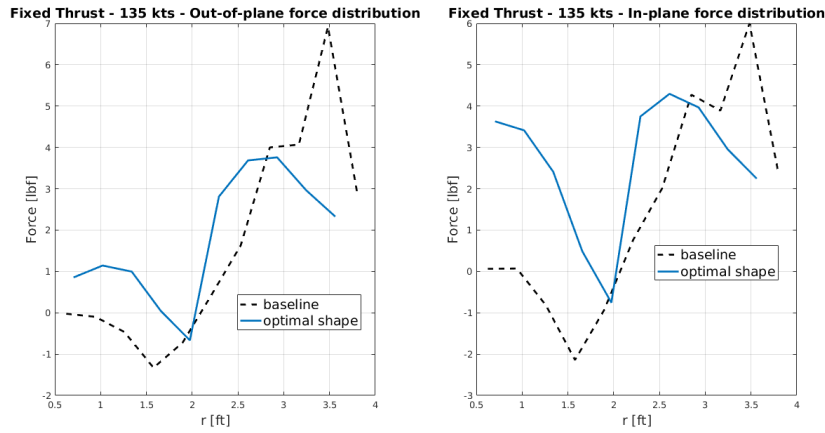
Figura 4.8: Forces acting on the blade at fixed thrust condition
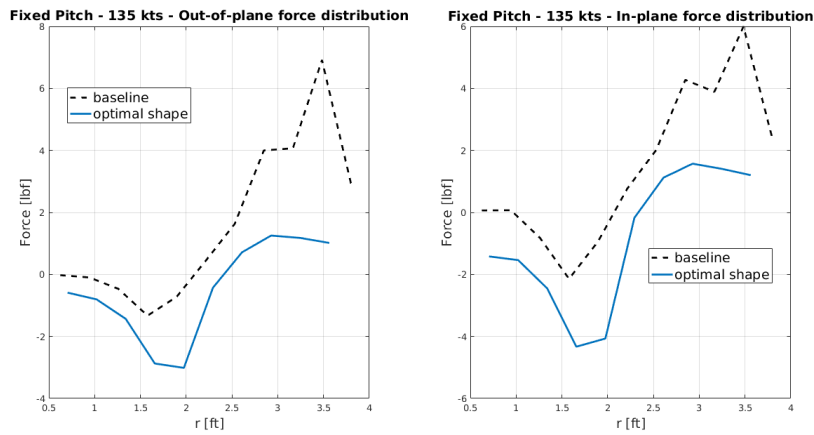
Figura 4.9: Forces acting on the blade at fixed pitch condition

The forces at fixed thrust are shown in figure 4.8. The optimal shape produces higher loads near the blade root with respect to the baseline. Instead the tip loads are lower. The position of the peaks is changed. the region of negative thrust is smaller and moved slightly toward the tip. Consequently the in-plane force produced by the optimal shape is higher, indeed the torque of the rotor is higher.

The thrust and the in-plane force at fixed pitch angle are shown in figure 4.9. It is well visible that the thrust is negative, indeed the out-of-plane force curve is negative up to $2.5 ft$. Also in this case, the trends of the two curves are different. The optimal shape withstands lower loads in the tip region. As expected also the in-plane force produced by the blade is negative, indeed the torque is negative as shown in table 4.3.

---

different.
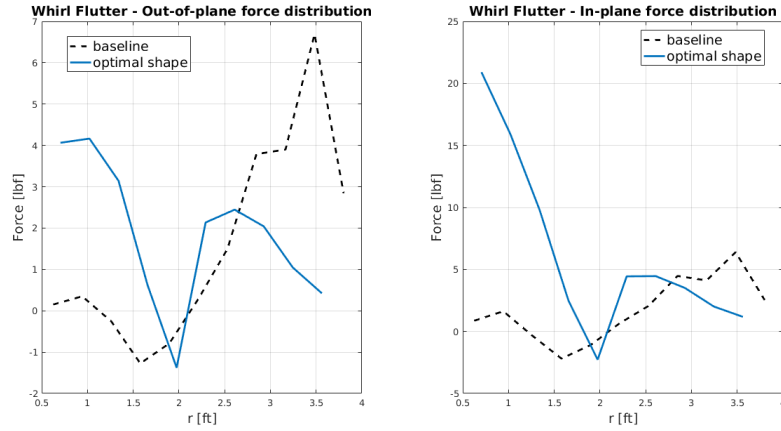
Figura 4.10: Forces acting on the blade at whirl flutter condition

Comparing the figures 4.8 and 4.9, it is possible to see how the introduction of the sweep decreases the thrust produced at the blade tip. Indeed, in this region the curve at fixed thrust has a more pronounced negative slope, that is the result of the elastic twist induced.

The comparison at the whirl flutter speed is shown in figure 4.10. The speeds of whirl flutter for the two model are different, however, the comparison helps to understand the differences that could modify the stability of the system. The figure 4.10 shows peculiar discrepancies. As shown previously, the optimal shape creates the majority of the thrust near the blade root. The tip region is almost unloaded. A large difference is evident in the two in-plane force curves. They cannot be compared in terms of absolute value because the two speed are very different, indeed the torque of the rotor with baseline blade is $177\,lbf\,ft$ and with the optimal blade is $269\,lbf\,ft$. The baseline model has a whirl flutter speed of $149kts$, while the optimal shape become unstable at $198kts$. However, the trends can be compared. The optimal blade produces high in-plane force near the root due to the evolution of the thrust produced, higher thrust produces higher drag. The relative low loads on the tip region of the blade help to increases the stability of the system.

Also in this case, it is clear that the introduction of aerodynamic modifications on the blades can increase the aeroelastic stability of the system with respect to whirl flutter. However, the responsible for the increment of damping is the elastic twist of the blade that inevitably increases the loads on the rotor hub and on the control chain. The higher torque generated by the rotor is the sum of two contribution, gurney flaps and the collective pitch correction. Airfoils equipped with gurney flaps have higher drag coefficient values increasing the torque. The collective pitch correction introduce hi-

gher angles of attack on the blade increasing the drag produced as well. The introduction of the sweep and so the twist of the blade modify the thrust distribution, decreasing the loads near the blade region but increasing them near the root.

Capitolo 5

Conclusions and future developments

The aims of the this work was to extend the whirl flutter boundaries of a tiltrotor model. The work done by Acree in [1] and [7] has been the basis for it. The present work has been focused on the aerodynamic modifications of the blade. The structure and twist changes have not been taken into account to simplify the analyses. A multibody semi-span tiltrotor model has been studied and used to assess the aeroelastic stability of the system. Four modification have been tested: gurney flaps, simple swept blades, double swept blades and blades with tip anhedral.

The use of gurney flaps to increase the whirl flutter speed has been proven and tested. In order to use the gurneys, a method to estimate the coefficients has been constructed. The method estimates some correction factors using wind tunnel tests. It has been developed in previous works and it has been extended in this work adding a method to construct the drag coefficient. The airfoil equipped with a 2%c gurney flap has been chosen for the current work. The wind tunnel tests show a negative slope of the pitching moment coefficient which means that, using a linear theory, there is a displacement of the aerodynamic center. The displacement has been calculated using the coefficient on the NACA 0012 equipped with the 2%c gurney flap. A parametric study of the application of gurney flaps on the blades of the tiltrotors has been done. A general increase of loads is associated with gurney flaps. However, a whirl flutter speed increment has been found. The increment of speed is about 14%, moving the limit from 149 to 170 kts but a growth in the power required has been noticed.

The use of swept blades increases the whirl flutter speed. However, the loads and the power required by this solution are high and could limit the implementation. A swept tip of 25° is capable of moving the whirl flutter speed of 20.8% with respect to the baseline. Some parametric studies have been done to understand the effects of sweeps. The loads, also in this case,

are higher than the baseline model. The increase of pitch link loads are significant. The first aeroelastic study of a double swept blade has been done. There is a general decrease of the whirl flutter speed even if high swept back tip angle is used. The blades with tip anhedral have been proven to be ineffective without considering the mass droop.

A more detailed description of the phenomena behind the use of blades with swept tip or equipped with gurney flaps has been done. The increase of speed is due to the elastic twist generated by the aerodynamic pitching moment along the blade. The stability of the system increases, however, the cost is an increase of the loads at the blade root, and, in particular, on the control chain and an increase of the power requirements. The flexibility of the blade and the pitch link are fundamental parameters for this peculiar phenomena.

An optimisation to increase the whirl flutter speed using double swept blades and gurney flaps has been set up and run. The optimal blade shape shows higher whirl flutter boundaries, however very high loads have been found. The optimal blade shows a whirl flutter speed increment of 32.9%.

All the studies in the present work have been done modifying only the aerodynamics of the blade. The structure has been kept unchanged to simplify the problem and the analyses. The introduction of the structure is the first development to be done. The use of swept blade and aeroelastic tailoring could increased the flight envelope of tiltrotors overcoming some loads limitations. The aeroelastic tailoring of the blade could be a solution to increase the boundaries keeping low loads and torque increments. The use of gurney flaps has been proven to increase the whirl flutter speed. The study could be extended using a device that can be extracted only in case of high speed flights in a passive way.

Appendice A

MBDyn

MBDyn is a general purpose Multibody Dynamics analysis software developed at the "Dipartimento di Scienze e Tecnologie Aerospaziali" of the University "Politecnico di Milano", Italy. MBDyn allows the simulation of multidisciplinary multibody systems. The multibody problem is formulated by directly writing the core equations for each unknown that can be structural, electric, hydraulic, etc. Consequently, it can simulate complex, non-linear systems like the model of the tiltrotor used here-in. The nature of the multi-field problems that can be formulated in MBDyn generates a system of Differential-Algebraic Equations (DAE) that must be solved using a proper A/L-stable algorithm (see [22] for the algorithm implemented).

A generic mechanical system can be described by a second order differential equation

$$\mathbf{M}(\mathbf{q})\ddot{\mathbf{q}} = \mathbf{f}(\dot{\mathbf{q}}, \mathbf{q}, t) \qquad (A.1)$$

where $\mathbf{q} \in \mathbb{R}^n$ are the n coordinates of the system, $\mathbf{M} \in \mathbb{R}^{n \times n}$ is the mass matrix and $\mathbf{f} : \mathbb{R}^{2n+1} \mapsto \mathbb{R}^n$ are the remaining forces that in general can be function of the dynamics of the system itself and of the time. The constraints are usually expressed using algebraic relationships between kinematic variables for holonomic constraints

$$\boldsymbol{\phi}(\mathbf{q}, t) = \mathbf{0} \qquad (A.2)$$

where $\boldsymbol{\phi} : \mathbb{R}^{n+1} \mapsto \mathbb{R}^c$ are the c equations that relates the coordinate of the system. In case of non-holonomic contraints the algebraic relationship in differential, non-integrable form is

$$\mathbf{A}(\mathbf{q}, t)\dot{\mathbf{q}} - \mathbf{b}(\mathbf{q}, t) = \mathbf{0}. \qquad (A.3)$$

where $\mathbf{A} \in \mathbb{R}^{c \times n}$ and $\mathbf{b} : \mathbb{R}^{n+1} \mapsto \mathbb{R}^c$. Actually the relation must be think as

$$\mathbf{A}(\mathbf{q}, t)d\mathbf{q} - \mathbf{b}(\mathbf{q}, t)dt = \mathbf{0} \qquad (A.4)$$

because the relationship is not integrable.

The constraints can be added to the uncontrained kinematic using Lagrangian's multipliers, $\boldsymbol{\lambda} \in \mathbb{R}^c$, that, in this context, represent the reaction forces. The augmented system with holonomic contraints is

$$
\begin{aligned}
\mathbf{M}(\mathbf{q})\ddot{\mathbf{q}} &= \mathbf{f}(\dot{\mathbf{q}}, \mathbf{q}, t) + \boldsymbol{\phi}_{,\mathbf{q}}^T \boldsymbol{\lambda} \\
\boldsymbol{\phi}(\mathbf{q}, t) &= \mathbf{0}
\end{aligned}
\tag{A.5}
$$

and with non-holonomic constraints

$$
\begin{aligned}
\mathbf{M}(\mathbf{q})\ddot{\mathbf{q}} &= \mathbf{f}(\dot{\mathbf{q}}, \mathbf{q}, t) + \mathbf{A}^T \boldsymbol{\lambda} \\
\mathbf{A}(\mathbf{q}, t)\dot{\mathbf{q}} - \mathbf{b}(\mathbf{q}, t) &= \mathbf{0}.
\end{aligned}
\tag{A.6}
$$

which are system of differential algebraic equations.

However, in MBDyn these equations are implemented in state space form

$$
\begin{aligned}
\mathbf{M}(\mathbf{q})\dot{\mathbf{q}} &= \mathbf{p} \\
\dot{\mathbf{p}} + \boldsymbol{\phi}_{,\mathbf{q}}^T \boldsymbol{\lambda} &= \mathbf{f}'(\dot{\mathbf{q}}, \mathbf{q}, \mathbf{p}, t) \\
\boldsymbol{\phi}(\mathbf{q}, t) &= \mathbf{0}
\end{aligned}
\tag{A.7}
$$

for system subject to holonomic constraint, and

$$
\begin{aligned}
\mathbf{M}(\mathbf{q})\dot{\mathbf{q}} &= \mathbf{p} \\
\dot{\mathbf{p}} + \mathbf{A}^T \boldsymbol{\lambda} &= \mathbf{f}'(\dot{\mathbf{q}}, \mathbf{q}, \mathbf{p}, t) \\
\mathbf{A}(\mathbf{q}, t)\dot{\mathbf{q}} - \mathbf{b}(\mathbf{q}, t) &= \mathbf{0}
\end{aligned}
\tag{A.8}
$$

for non-holonomic constraints, where $\mathbf{p}$ are the momentum and momenta moments and $\mathbf{f}' : \mathbb{R}^{3n+1} \mapsto \mathbb{R}^c$ are the remaining forces expressed in the state space form.

The problem as formulated in A.8 is solved used the aforementioned algorithm for every time step.

Appendice B

Strip Theory

There are numbers of different ways to model the spanwise lift distribution of an aerodynamic surface. Strip theory is the simple one and gives good results in a relative low amount of time with respect to more sophisticated methods. In strip theory, the wing or the blade (in general an aerodynamic surface) is considered composed of a number of elemental chordwise "strips" of finite width Δy, also called sections.

The lift is calculated as the summation of the contribution of every single strip. It is assumed that the lift coefficient on each chordwise section of the aerodynamic surface is proportional to the local angle of attack and the local freestream velocity as well. Every strip has no influence on the other one. Consider an elemental strip "k", the sectional lift is taken to act at its aerodynamic centre (i.e. quarter chord) and is defined as

$$L_k = \frac{1}{2}\rho V_k^2 c_k \Delta y_k C_{L_k} \tag{B.1}$$

where all the local quantities are used, V_k is the local freestream velocity, c_k is the local chord, Δy_k is the section span and, C_{L_k} is the local lift coefficient. In order to have a more sophisticated result, MBDyn uses lookup tables to provide the aerodynamic coefficients. MBDyn enters in the table with the local angle of attack computed using the local airflow (composed by the freestream speed plus the velocity given by the inflow model specified), and the local displacement of the aerodynamic element.

The theory does not take into account the drag and the pitching moment produced, however, the use of lookup tables gives the possibility to overcome this strong limitation. The drag does not contain directly three dimensional effects. The finite dimensionality of the aerodynamic surface has to be introduced using the proper inflow model. Strip theory as it has been constructed does not give the possibility to study swept lifting surfaces and more complicated geometries, however, it can be modified in order to take into account the effects of displacement of the aerodynamic center. The

unsteadiness of the flow can be introduced using simplified theories such as Theodorsen's one.

In this way is possible to use the strip theory also in more complicated conditions keeping a simple and economic way to introduce aerodynamic calculations in fluid-structure interaction problems.

Appendice C

Validation panel displacements

In order to validate the fact that moving the overall aerodynamic panel is equivalent to changing the aerodynamic center locus using the tools provided by MBDyn different tests have been done. Only one of these is reported here. The simple swept blade with $\lambda_2 = 25°$ has been used. The two different configurations are reported in figure C.1. The sections are moved using the interpolation point of the aerodynamic center line corresponding to a deflection angle as defined in figure, and the mid chord line of the semi panel.

The two blades have been tested in several conditions. Like the other comparisons done in the present work, the speed has been fixed at $135kts$ and two different trim conditions have been used: fixed thrust and fixed pitch. Then, the whirl flutter conditions have been checked as well.

The results at fixed thrust conditions are reported in table C.1. As visible, the results are perfectly comparable.

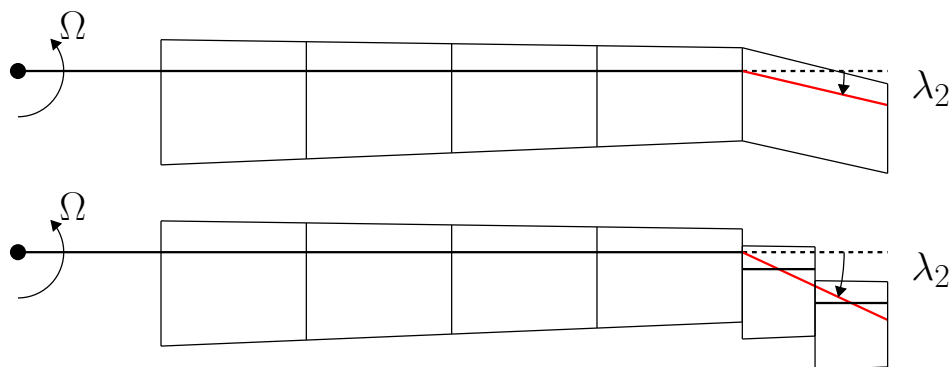Instead, the fixed pitch results are reported in table C.2. Also in this

Figura C.1: Linear aerodynamic center line vs. piecewise constant displacement

Sweep type	Flap moment [lbf ft]	Lag moment [lbf ft]	Pitch link load [lbf]	Thrust [lbf]	Torque [lbf ft]	Coning angle [°]	Pitch variation [°]
linear line	3.35	49.50	13.65	51.20	165.60	2.26	1.90
moving panels	3.33	49.17	13.70	51.18	165.43	2.22	1.90

Tabella C.1: Summary validation at fixed thrust for $\lambda_2 = 25°$

Sweep type	Flap moment [lbf ft]	Lag moment [lbf ft]	Pitch link load [lbf]	Thrust [lbf]	Torque [lbf ft]	Coning angle [°]	Pitch variation [°]
linear line	10.90	14.60	12.06	12.32	50.45	1.10	0.00
moving panels	10.88	14.63	12.08	12.36	50.54	1.12	0.00

Tabella C.2: Summary validation at fixed pitch for $\lambda_2 = 25°$

case the values are comparable, and in general, the loads are sensibly higher moving all the sections. Also the coning angle is slightly reduced.

Looking the previous values the expectation for the whirl flutter speed are good. The results confirm the expectations, see table C.3, the whirl flutter speed is the same for both the models as well as the collective pitch used to hold the thrust value.

Due to the strip theory where every panel has not influence on the other one, varying the aerodynamic center line or moving the panel itself produces the same result.

Sweep type	Whirl flutter speed	$\Delta\theta_0$
linear line	$180kts$	$+1.90°$
moving panels	$180kts$	$+1.90°$

Tabella C.3: Summary validation at whirl flutter speed

Bibliografia

[1] C.W. Acree Jr., RJ Peyran, and Wayne Johnson. Rotor design for whirl flutter: An examination of options for improving tiltrotor aeroelastic stability margins. Technical report, NATIONAL AERONAUTICS AND SPACE ADMINISTRATION MOFFETT FIELD CA AMES RESEARCH CENTER, 1999.

[2] CW Acree Jr, RJ Peyran, and Wayne Johnson. Rotor design options for improving xv-15 whirl-flutter stability margins. Technical report, NATIONAL AERONAUTICS AND SPACE ADMINISTRATION MOFFETT FIELD CA AMES RESEARCH CENTER, 2004.

[3] Shirley M Barkai and Omri Rand. The influence of composite induced couplings on tiltrotor whirl flutter stability. *Journal of the American Helicopter Society*, 43(2):133–145, 1998.

[4] Olivier A Bauchau and Jielong Wang. Stability analysis of complex multibody systems. *Journal of Computational and Nonlinear Dynamics*, 1(1):71–80, 2006.

[5] Richard L. Bielawa. *Rotary wing structural dynamics and aeroelasticity.* 2006.

[6] Raymond L Bisplinghoff, Holt Ashley, and Robert L Halfman. *Aeroelasticity.* Courier Corporation, 2013.

[7] Acree Jr. C. Effects of swept tips on v-22 whirl flutter and loads. Technical report, Ames Research Center, Moffett Field, California, 2005.

[8] Giovanni Droandi. *Wing-rotor aerodynamic interaction in tiltrotor aircraft.* PhD thesis, 2014.

[9] Gian Luca Ghiringhelli, Pierangelo Masarati, and Paolo Mantegazza. Multibody implementation of finite volume c beams. *AIAA journal*, 38(1):131–138, 2000.

[10] Gian Luca Ghiringhelli, Pierangelo Masarati, Paolo Mantegazza, and Mark W Nixon. Multi-body analysis of a tiltrotor configuration. *Nonlinear Dynamics*, 19(4):333–357, 1999.

[11] Edward Lewis Houghton and Peter William Carpenter. *Aerodynamics for engineering students*. Butterworth-Heinemann, 2003.

[12] David Jeffrey, Xin Zhang, and David W Hurst. Aerodynamics of gurney flaps on a single-element high-lift wing. *Journal of Aircraft*, 37(2):295–301, 2000.

[13] Wayne Johnson. *Rotorcraft aeromechanics*, volume 36. Cambridge University Press, 2013.

[14] Taeseong Kim, Jaehoon Lim, SangJoon Shin, and Do-Hyung Kim. Structural design optimization of a tiltrotor aircraft composite wing to enhance whirl flutter stability. *Composite Structures*, 95:283–294, 2013.

[15] Taeseong Kim and SangJoon Shin. Advanced analysis on tiltrotor aircraft flutter stability, including unsteady aerodynamics. *AIAA journal*, 46(4):1002–1012, 2008.

[16] Gordon J Leishman. *Principles of helicopter aerodynamics with CD extra*. Cambridge university press, 2006.

[17] Yachen Li, Jinjun Wang, and Panfeng Zhang. Effects of gurney flaps on a naca0012 airfoil. *Flow, Turbulence and Combustion*, 68(1):27–39, 2002.

[18] Yachen Li, Jinjun Wang, and Panfeng Zhang. Influences of mounting angles and locations on the effects of gurney flaps. *Journal of Aircraft*, 40(3):494–498, 2003.

[19] Robert H Liebeck. Design of subsonic airfoils for high lift. *Journal of aircraft*, 15(9):547–561, 1978.

[20] Tianshu Liu and Javier Montefort. Thin-airfoil theoretical interpretation for gurney flap lift enhancement. *Journal of Aircraft*, 44(2):667–671, 2007.

[21] Pierangelo Masarati. *MBDyn Input File Format, Version 1.7.2*, 2017.

[22] Pierangelo Masarati, Massimiliano Lanz, and Paolo Mantegazza. Multistep integration of ordinary, stiff and differential-algebraic problems for multibody dynamics applications. In *XVI Congresso Nazionale AIDAA, pages*, volume 71, 2001.

[23] Pierangelo Masarati and Marco Morandini. An ideal homokinetic joint formulation for general-purpose multibody real-time simulation. *Multibody System Dynamics*, 20(3):251–270, 2008.

[24] Pierangelo Masarati, David J Piatak, Giuseppe Quaranta, Jeffrey D Singleton, and Jinwei Shen. Soft-inplane tiltrotor aeromechanics investigation using two comprehensive multibody solvers. *Journal of the American Helicopter Society*, 53(2):179–192, 2008.

[25] Mattia Mattaboni. *Aeroelastic modeling and active control of tiltrotor aircraft.* PhD thesis, 2011.

[26] Mattia Mattaboni, Pierangelo Masarati, Giuseppe Quaranta, and Paolo Mantegazza. Multibody simulation of integrated tiltrotor flight mechanics, aeroelasticity and control. *Journal of Guidance, Control and Dynamics*, 2012.

[27] Mark W Nixon, David J Piatak, Lawrence M Corso, and David A Popelka. Aeroelastic tailoring for stability augmentation and performance enhancements of tiltrotor aircraft. *Journal of the American Helicopter Society*, 45(4):270–279, 2000.

[28] David J Piatak, Raymond G Kvaternik, Mark W Nixon, Chester W Langston, Jeffrey D Singleton, Richard L Bennett, and Ross K Brown. A parametric investigation of whirl-flutter stability on the wrats tiltrotor model. *Journal of the American Helicopter Society*, 47(2):134–144, 2002.

[29] Rupinder Singh, Farhan Gandhi, Jinho Paik, and Eric Hathaway. Active tiltrotor whirl-flutter stability augmentation using wing-flaperon and swash-plate actuation. *Journal of Aircraft*, 44(5):1439–1446, 2007.

[30] SN Sivanandam and SN Deepa. *Introduction to genetic algorithms.* Springer Science & Business Media, 2007.

[31] Venkataraman Srinivas, Inderjit Chopra, and Mark W Nixon. Aeroelastic analysis of advanced geometry tiltrotor aircraft. *Journal of the American Helicopter Society*, 43(3):212–221, 1998.

[32] Lance W Traub. Prediction of gurney-flap lift enhancement for airfoils and wings. *AIAA Journal*, 52(9):2087–2090, 2014.

[33] JJ Wang, YC Li, and K-S Choi. Gurney flap—lift enhancement, mechanisms and applications. *Progress in Aerospace Sciences*, 44(1):22–47, 2008.

[34] Reed III W.H. Propeller-rotor whirl flutter: a state-of-art review. Technical report, NASA Langley Research Center, Langley Station, Hampton, Va., U.S.A., 1965.

[35] Kwanjung Yee, Wandon Joo, and Dong-Ho Lee. Aerodynamic performance analysis of a gurney flap for rotorcraft application. *Journal of Aircraft*, 44(3):1003–1014, 2007.